U.S. Department of Commerce
National Oceanic and Atmospheric Administration
National Weather Service
National Centers for Environmental Prediction
5830 University Research Court
College Park MD 20740-3818

Office Note 511
https://doi.org/10.25923/5fyz-rb36

Updates to RAS Version 2 and its Application to the NOAA Unified Forecast System

Shrinivas Moorthi
NOAA/NWS/NCEP Environmental Modeling Center

November 2022

E-mail: Shrinivas.Moorthi@noaa.gov

Abstract

In this report an advanced and improved version of the Relaxed Arakawa-Schubert (RASv2) convection parameterization, originally developed by Moorthi and Suarez (1992,hereafter MS92, 1999, hereafter MS99) is presented. MS99 included several important improvements of the original RAS presented in MS92. The cloud model in MS99 accounts for virtual effects of moisture in the buoyancy calculations and includes suspended cloud condensate loading and autoconversion at various levels, producing precipitation as a function of height. The suspended cloud condensate is detrained at the cloud-top. This detrained cloud condensate is the convective source of environmental cloud condensate which is needed for models with prognostic cloud condensate. A simple treatment of the ice phase has also been added.

MS99 also includes a scheme for the evaporatively driven convective downdraft following Cheng and Arakawa (1997a,b) and a scheme to account for the evaporation of the falling rain that does not generate downdrafts following Sud and Molod (1988).

Nevertheless, MS99 had some typographical errors and a fortran bug in the semi-prognostic test that made the results noisy. Therefore, I will present here corrected version with some repetition of MS99 for completeness, but with improved results.

Single Column Model (SCM) results using National Center's for Environmental Prediction (NCEP) SCM for the GATE data is also presented and compared against the original RASV1. Results show that the performance of RASv2 is superior that of RASv1 in SCM simulations for GATE.

Additionally I will present updates to use quasi-positive-definite advection of the environmental condensates via compensating subsidence in the environment. Some results from the applicaiton of RASv2 in coupled/uncoupled NOAA Unified Forecast System (UFS) areis also presented.

1 Introduction

Cumulus convection plays a dominant role in both the thermodynamical and the hydrological cycles of the earth's atmosphere. Accurate prediction of heat and moisture changes in the atmosphere due to cumulus convection is crucial to the success of numerical weather prediction, as well as to climate and global change studies. The most elegant and complete theory of the interaction between cumulus ensembles and the large-scale environment is presented in the pioneering work of Arakawa and Schubert (1974, hereafter AS), and has remained so for over two decades. Nevertheless, the standard implementation of this theory in weather prediction and climate models (e.g., Lord et al., 1982) is quite expensive, particularly when the vertical resolution is high. This has limited the application of the AS scheme.

The AS parameterization assumes that convection will act to maintain the atmospheric sounding in a state of "quasi-equilibrium" in which the tendency of other (slower) processes to destabilize the sounding are closely compensated by the tendency of the convection to stabilize it. In AS the assumption that this state is obtained at each instant, together with some simple assumptions about the interactions between individual clouds and the environment—the so-called "cloud model"—is sufficient closure to compute the vertical profiles of heating and moistening due to the effects of convection. AS expects this adjustment to quasi-equilibrium occur quickly compared to changes in the destabilizing effects of the large-scale flow.

Moorthi and Suarez (1992, hereafter, MS92) developed the relaxed Arakawa-Schubert (RAS) scheme (hereafter referred to as RASv1), which is a simple and economical implementation of the basic ideas of AS. It is based on the notion that the adjustment required by AS can be effected in a finite time. In developing RASv1, MS92 made several simplifications, both in the cloud model and in the manner in which quasi-equilibrium is achieved. The cloud model was simplified by assuming that the normalized cloud updraft mass flux is a linear function of height and by ignoring the effects of cloud condensate loading and moisture content in the buoyancy calculations. The quasi-equilibrium is achieved through an iteration that "relaxes" the sounding toward the equilibrium state in a prescribed time, instead of simultaneously letting all

cloud ensembles adjust the environment to a state of equilibrium (as in the AS implementation). The iteration is performed by adding at each step the effects of a single cloud type. In practice, this is achieved by invoking several cloud types every time step, one by one, and letting a fraction (the relaxation parameter) of the mass flux required for full quasi-equilibrium modify the environment. Thus, the computation of effects of these individual cloud types is the core of the RAS calculation.

RASv1 has been quite successful in achieving its original goals of economy and simplicity while retaining the essence of AS, and some form of it has been used at several institutions. However, as in the original implementation of AS, it suffers from excessive drying due to the lack of downdraft effects as well as to a lack of evaporation of falling rain in the environment. A method for reducing the excessive drying was proposed by Sud and Molod (1988) in their implementation of AS. Moorthi (2000) included a simplified version of the Sud and Molod scheme for evaporation of falling convective rain to alleviate this excessive dry and warm bias in the RASv1 and this version is being used in the NCEP Climate Prediction Center's climate model. Sud and Walker (1999a,b) developed a methodology to couple microphysics of clouds with RAS and included a downdraft scheme based on Sud and Walker (1993).

Moorthi and Suarez (1999, hereafter MS99) documented an advanced version of RAS (hereafter RASv2) in which several simplifications made in the RASv1 were removed. Major changes were in the cloud updraft model which included a budget of condensed water within the clouds. MS99 included the condensate loading, the virtual effect of water vapor, and allowed for the normalized mass flux to be a quadratic function of height to alleviate problems associated with the linear mass flux used in MS92, and included a simple ice phase. These additions gave a fairly complete implementation of the AS updraft cloud model which greatly facilitates the coupling of the updraft to downdraft and stratiform cloud schemes.

MS99 also presented a downdraft formiulation based on Cheng and Arakawa (1997a, 1997b, hereafter CA97a and CA97b). In this implementation, the downdrafts are driven by precipitation loading and evaporation and can be saturated or unsaturated. The precipitation flux that is available for the downdraft is obtained as a steady state solution of a tilted updraft. Thus, the precipitation need not be available for

the downdraft at the level where it is generated, and can be vertically advected within the updraft. Downdrafts can start and end anywhere in the vertical domain. However, both the scheme for the determination of the available rain flux from the updraft and the calculation of the downdraft properties are computationally intensive. Nevertheless, we have incorporated a version of this downdraft scheme with some approximations in the present version of RAS.

Detailed documentation of RASv2 was provided in MS99. Here slightly updated version of RASv2 with some corrections (with some repetetion for completeness) is presented. The organization of this document is as follows. In Section 2 some basic relations are reviewed. Details of the cloud updraft model are in section 3 followed by the adaptation of Cheng and Arakawa (hereafter, CA) downdraft scheme in section 4. Semi-prognostic evaluation using GATE Phase III datai are presented in section 6. A strategy for application of the parameterization to numerical models of the atmosphere with high vertical resolution is presented in Section 7. SCM results are presented in Section 8. Recent updates to RASv2 such as quasi-positive definite vertical advection of environmental tracers (including suspended cloud condensates) and implemenmtation of simple scale awareness (Arakawa-Wu, 2013, Han et al., 2017). Some results from application to coupled/uncoupled NOAA UFS are presented in section 9 A summary is provided in Section 10. Discrete formulation of the parameterization is provided in the Appendix.

2 Basic Relations

Treating moist air as an ideal gas, the equation of state is

$$p = \left(\frac{\rho_d}{\mu_d} + \frac{\rho_{\rm v}}{\mu_{\rm v}} \right) R^* T = \rho R_d T_{\rm v}, \tag{1}$$

where p is the pressure, $\mu_d = 28.97$ and $\mu_{\rm v} = 18.016$ are the molecular weights of dry air and water vapor, R^* is the universal gas constant, $R_d = \frac{R^*}{\mu_d}$ is the gas constant for dry air, ρ_d and $\rho_{\rm v}$ are the densities of dry air and water vapor, $\rho = \rho_d + \rho_{\rm v}$ is the

density of the moist air, T is the temperature, and

$$T_{\rm v} = [1 + (\frac{\mu_d}{\mu_{\rm v}} - 1)q\,]\,T = (1 + \nu q)\,T \tag{2}$$

is the virtual temperature, $q = \frac{\rho_{\rm v}}{\rho}$ being the specific humidity. We have defined the constant $\nu \equiv (\frac{\mu_d}{\mu_{\rm v}} - 1) \approx 0.608$.

In RASv2 also we use the same form of the hydrostatic equation as the Arakawa and Suarez (1983) scheme, but with virtual effects of moisture:

$$d\phi = -\theta_{\rm v}\, d\Pi, \tag{3}$$

where $\phi = gz$ is the geopotential, z is height, g is the acceleration of gravity, $\theta_{\rm v} = c_p \frac{T_{\rm v}}{\Pi}$ is the virtual potential temperature, $\Pi = c_p \left(\frac{p}{p_0}\right)^{\kappa}$ is the Exner function, p_0 is a reference pressure, c_p is the specific heat of dry air at constant pressure, and $\kappa = R_d/c_p$.

We define the dry static energy, s, the moist static energy, h, and the saturated moist static energy, h^*, as

$$s = c_p T + \phi, \tag{4a}$$

$$h = s + L_c q, \tag{4b}$$

$$h^* = s + L_c q^*, \tag{4c}$$

where L_c is the latent heat of condensation of water vapor, which is assumed to be a constant, and $q^* = q_{sat}(T, p)$ is the saturation specific humidity. The dry static energy is conserved during a dry adiabatic process, and the moist static energy is conserved during a pseudo-adiabatic process not involving the ice phase. When the ice phase is involved, a generalized moist static energy defined as

$$h = s + L_c q - L_f q^I \tag{5}$$

is conserved (Lord, 1978), where q^I is the ice water mixing ratio, and L_f is the latent heat of fusion of water. Another conservative quantity is the total water, q^T, defined as

$$q^T = q + q^L + q^I, \tag{6}$$

where q^L is the liquid water mixing ratio. In the present formulation of RAS we allow for ice phase condensate by using a simple partitioning similar to that used by Lord (1978). Thus we approximate

$$q^I = Q(T)q^C \tag{7}$$

where $q^C = q^L + q^I$ is the total condensate, and $Q(T)$ is a temperature dependent function, defined as

$$Q(T) = \frac{T_L - T}{T_L - T_F} \tag{8}$$

where $T_L = -263.16\ K$, $T_F = -233.16\ K$, and $0 \leq Q \leq 1$ is required. In Lord (1978), T was taken as the temperature of the cloud air, but for simplicity we use the environmental temperature.

The virtual dry static energy $s_{\rm v}$ is defined as

$$s_{\rm v} = s + c_p T(\nu q - q^L - q^I). \tag{9}$$

It will be convenient also to define the quantity

$$\gamma = \frac{L_c}{c_p}\frac{\partial q^*}{\partial T}(T, p). \tag{10}$$

3 The Updraft Cloud Model

Deep cumulus clouds are assumed to consist of a saturated updraft, possibly accompanied by a downdraft. The entire cloud is assumed to occupy a small horizontal area. Subsidence that exactly compensates the net updraft and downdraft mass fluxes is assumed to occur uniformly in the large-scale environment outside the cloud. This subsidence produces the heating and drying effects of the clouds on the environment. In this section we discuss the updraft model.

3.1 Updraft Properties

The updraft mass flux, M^u, is written as

$$M^u(z) = M_B\, \eta^u(z), \tag{11}$$

where M_B is the mass flux entering the updraft at cloud base, z_B, and $\eta^u(z)$ is the normalized mass flux as a function of height; obviously, $\eta^u(z_B) = 1$. (We will use the superscript "u" to denote updraft properties. The absence of a superscript indicates environmental properties.) Within the updraft, the divergence of the flux of conservative quantities must equal the entrainment flux. Mass conservation is thus written as

$$d\eta^u = \mathcal{E}\, dz, \tag{12}$$

where $\mathcal{E}$ is the normalized lateral mass entrainment per unit height. Using the generalized moist static energy, h, and total water, q^T, as the two conservative thermodynamic quantities, we write

$$d(\eta^u h^u) = h\mathcal{E}\, dz = h\, d\eta^u, \tag{13}$$

for the moist static energy budget, and

$$d(\eta^u q^{uT}) = q^T \mathcal{E}\, dz - \mathcal{R}\, dz = q^T\, d\eta^u - \mathcal{R}\, dz, \tag{14}$$

for the total water budget, where h and q^T represent moist static energy and total water in the environment, $\mathcal{R}$ is the precipitation production rate per unit height normalized by M_B, and

$$h^u = c_p T^u + \phi + L_c q^u - L_f q^{uI} \tag{15}$$

is the generalized moist static energy in the cloud updraft, where

$$q^u = q^{uT} - q^{uL} - q^{uI}. \tag{16}$$

Here q^u, q^{uT}, q^{uL}, and q^{uI} are the cloud updraft specific humidity, total water, liquid water mixing ratio, and ice mixing ratio, respectively. In (13) and (14) we have assumed that all lateral entrainment into the updraft is from the environment and none is from the associated downdraft. The total water in the entrained air is $q^T = q + q^L + q^I$ if the environment contains suspended liquid water and/or ice. Integrating (13) and (14) gives

$$\eta^u(z) h^u(z) = h_B + \int_{z_B}^{z} h(z') \frac{d\eta^u}{dz'}\, dz', \tag{17}$$

and

$$\eta^u(z) q^{uT}(z) = q_B + \int_{z_B}^{z} q^T(z') \frac{d\eta^u}{dz'}\, dz' - \int_{z_B}^{z} \mathcal{R}\, dz', \tag{18}$$

since the subcloud layer is assumed to be unsaturated. Here z is height and the subscript "B" represents values at the top of the subcloud layer.

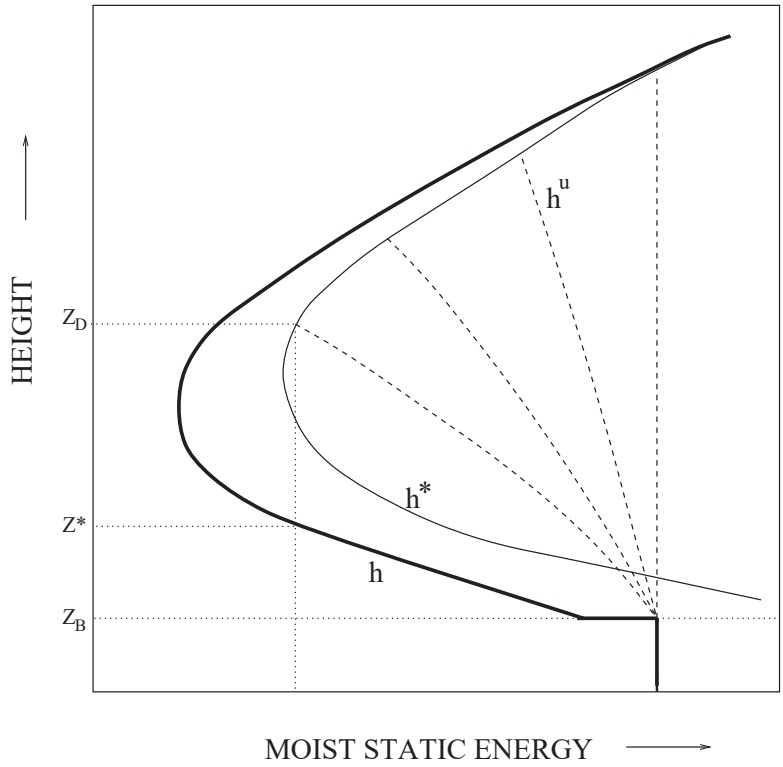

Figure 1: Schematic of the moist static energy distributions.

Figure 1 shows schematically the vertical profile (thick solid line) of moist static energies that occur typically in a conditionally unstable sounding. The subcloud layer is shown as a mixed layer with constant h. The sounding is unsaturated everywhere, with $h < h^*$. The dashed lines show four possible distributions of updraft moist static energy, h^u, corresponding to four different rates of entrainment. As can be seen from (17), $h^u(z)$ is a weighted average of the h in the subcloud layer and in the environment at levels below z.

3.2 The Entrainment Relation

In the AS parameterization, cloud types are characterized completely by their rate of lateral entrainment. The higher the rate of entrainment, the closer h^u is to the environmental value h, and as can be seen from figure 1, the lower the level at which $h^u = h^*$. This is approximately the level of non-buoyancy and usually assumed to be the cloud top. A higher entrainment rate thus implies shallower clouds.

As is standard practice, AS use the entrainment relation

$$\frac{1}{\eta^u}\frac{d\eta^u}{dz} = \lambda, \tag{19}$$

where λ is the entrainment parameter used to characterize each cloud type. Integrating (19) gives $\eta^u(\zeta) = e^{\lambda\zeta}$, where $\zeta = (z - z_B)$. In MS92 this relation was simplified to $\eta^u(\zeta) = 1 + \lambda\zeta$, which approximates the exponential only for small $\lambda\zeta$ and implies constant entrainment per unit height in the vertical. Arakawa and Cheng (1993) noted that this approximation systematically reduces the occurrence of soundings that can support middle level cloud types, whose detrainment level is near the level of minimum h and h^*. To understand why this is, we again refer to figure 1. If we consider the lowest of the four cloud types shown, which detrains at level z_D, we see that the moist static energy in the cloud at cloud top must be near $h^*(z_D)$ and must be obtained through a mixture of the air below z_D. But note that only the relatively small region between z_D and z^* can contribute values of h lower than $h^*(z_D)$; while the larger region below z^* contributes air with moist static energies greater than $h^*(z_D)$, particularly if the lower atmosphere is relatively moist. For linear entrainment, as assumed in MS92, these two contributions would receive roughly equal weight. As a result, it is virtually impossible to find a λ that yields $h^u(z_D) \approx h^*(z_D)$. In fact, h^u at any level below the minimum in h^* cannot be less than the height-averaged environmental h between that level and cloud base. For entrainment that increases exponentially with height, the upper contribution could receive a much greater weight, and it would thus be more likely that a λ could be found that produces a mixture yielding $h^u(z_D) \approx h^*(z_D)$. Thus, entrainment that rapidly increases with height is essential for the existence of shallow cloud types.

To more closely approximate the behavior of the original AS scheme, while retaining most of the efficiency of the linear η^u relation, the new version of RAS uses a quadratic relation:

$$\eta^u(\zeta) = 1 + \lambda\zeta + \frac{1}{2}(\lambda\zeta)^2. \tag{20}$$

As we shall see below, this can be implemented with little additional calculation.

3.3 Buoyancy and the Cloud Work Function

In RASv2, we use a more precise calculation of the buoyancy of the updraft than used in MS92, including virtual effects and loading by suspended cloud condensate (both water and ice, but not rain). [1] The acceleration due to buoyancy of an updraft parcel consisting of a mixture of moist air and suspended condensed water is

$$B^u = -g\frac{\rho^u - \rho}{\rho^u} - g[q^{uL} + q^{uI} - q^L - q^I], \tag{21}$$

where ρ^u is the density of moist air within the updraft and ρ is the density of moist air in the environment.

Using (1) and neglecting density variations due to pressure differences between the updraft and the environment, the buoyancy can be accurately approximated by

$$B^u = g\left[\frac{T_{\rm v}^u - T_{\rm v}}{T_{\rm v}} - q^{uL} - q^{uI} + q^L + q^I\right]. \tag{22}$$

Now

$$T_{\rm v}^u - T_{\rm v} = (T^u - T)(1 + \nu q^*) + \nu T(q^u - q^*) + \nu T(q^* - q) + \nu(T^u - T)(q^u - q^*). \tag{23}$$

Ignoring the last quadratic term and using the following approximate relations

$$T^u - T = \frac{1}{c_p(1+\gamma)}[h^u + L_f q^{uI} - h^*], \tag{24}$$

and

$$q^u - q^* = \frac{\gamma}{L_c(1+\gamma)}[h^u + L_f q^{uI} - h^*], \tag{25}$$

[1] The impact of precipitation within the updraft itself would be to reduce the updraft buoyancy thus inhibiting the cloud's growth and leading to its destruction. Nevertheless, we do not take into account this drag in calculating the buoyancy of the updraft.

which are valid for a saturated parcel, we can write the buoyancy above the condensation level in the form

$$B^u = \frac{g}{\tilde{L}}\left[h^u + L_f q^{uI} - h^{**} - \tilde{L}(q^{uL} + q^{uI} - q^L - q^I)\right], \tag{26}$$

where, similarly to CA97b, we have defined a grid-scale virtual moist static energy h^{**} as

$$h^{**} = h^* - \frac{\nu\tilde{L}}{(1+\nu q)}[q^* - q], \tag{27}$$

and

$$\tilde{L} = \frac{(1+\gamma)c_p T_{\rm v}}{(1+\gamma\nu c_p T/L + \nu q^*)}. \tag{28}$$

Below the condensation level, the buoyancy can be approximated by

$$B^u = \left[\frac{(s^u - s)}{c_p T_{\rm v}} + \nu(q^u - q) + q^L + q^I\right]. \tag{29}$$

Following AS, we define the cloud work function as the work done by thermal buoyancy of the updraft per unit cloud-base mass flux:

$$\mathcal{A} \equiv \int_{z_B}^{z_D} \eta^u(z) B^u(z)\, dz. \tag{30}$$

Here z_D is the height of the cloud top. CA97a provided alternate definitions of the cloud work function for combined updraft-downdraft models by taking into account rain-water drag on updraft, and thermal buoyancy and rain-water drag in the downdraft. CA97a showed that despite the differences in magnitude of the cloud work function with these alternate definitions, they are proportional to each other and that using the definition (30) in implementing cloud work function quasi-equilibrium is acceptable. Following CA97a, we also use (30) in our implementation, since this results in significant savings in computations.

Combining (30) with (29) and (26) gives

$$\begin{aligned}\mathcal{A} \;\approx\; & g\int_{z_B}^{z_C}\left[\frac{(s^u - s)}{c_p T_{\rm v}} + \nu(q^u - q) + q^L + q^I\right]\eta^u(z)\, dz \\ & + g\int_{z_C}^{z_D}\frac{1}{\tilde{L}}\left[h^u + L_f q^{uI} - h^{**} - \tilde{L}(q^{uL} + q^{uI} - q^L - q^I)\right]\eta^u(z)\, dz, \end{aligned} \tag{31}$$

where z_C is the condensation level.

3.4 Entrainment Parameter and the Cloud Condensate Budget

Updraft properties can be determined if the entrainment parameter characterizing the cloud type is known. The entrainment parameter is determined assuming nonbuoyancy condition at the cloud top. If the cloud updraft detrains at the cloud top level, z_D, then using the form of the buoyancy that appears in the integrand of (31) for levels above z_C, the nonbuoyancy condition at the cloud top can be obtained as

$$h^u(z_D) + L_f q^{uI}(z_D) - h^{**}(z_D) - \tilde{L}\left[q^{uC}(z_D) - q^C(z_D)\right] = 0 \tag{32}$$

This relation involves only three updraft quantities, h^u, q^{uC} and q^{uI}, all evaluated at the detrainment level. The moist static energy h^u can be obtained from (17). The cloud condensate mixing ratio $q^{uC} = q^{uL} + q^{uI}$ can be obtained from (18) after proper parameterization of precipitation production rate $\mathcal{R}$. Cloud ice mixing ratio can be computed from q^{uC} using (7). As mentioned before, the environmental temperature T is used in evaluating $Q(T)$ instead of updraft temperature T^u. Without this approximation, the entrainment parameter can only be determined iteratively. Since the updraft air is typically a few degrees warmer than the environmental air, the above approximation overestimates the ice fraction in the total condensate mixing ratio. A crude adjustment can be made by reducing T_L and T_F in (8) by a few degrees. Nevertheless, we do not expect the error due to this approximation to be of significance since the choice of $Q(T)$ itself is perhaps not very accurate.

The precipitation production rate $\mathcal{R}$ is generally parameterized as

$$\begin{aligned} \mathcal{R} &= c_0 \eta^u(z)\left[q^{uC}(z) - q_0\right], \text{ if } q^u(z) > 0 \\ &= 0 \text{ if } q^u(z) \le 0 \end{aligned} \tag{33}$$

where c_0 is the auto conversion coefficient, and q_0 is a critical cloud condensate mixing ratio, which can be different for water and ice. Then the differential equation governing the vertical distribution of the condensate can be written as

$$\frac{d(\eta^u q^{uC})}{dz} + \mathcal{R} = q^T(z)\frac{d\eta^u}{dz} - \frac{d(\eta^u q^u)}{dz}. \tag{34}$$

For a nonzero q_0, the definition of $\mathcal{R}$ as in (33) requires iterative solution of the nonbuoyancy condition to determine the entrainment parameter. To avoid this complication, Moorthi and Suarez (1999) chose $q_0 = 0$, which makes the direct solution of λ possible. In this case it is possible to obtain the suspended cloud condensate at any level in the form

$$\eta^u(z)q^{uC}(z) = \lambda^2 F(z) + \lambda G(z) + H(z), \tag{35}$$

where F, G, and H are vertical integrals depending on environmental variables only (See MS99 for details for the discrete case). While Aakawa and Schubert (1974) chose $q_0 = 0$, Cheng and Arakawa (1998) use $q_0 = 0.001$ kg/kg for ice and $q_0 = 0.0$ kg/kg for water (although they are proposing to use $q_0 = 0.0007$ kg/kg for water in the future).

To avoid iterative solution, here we adopt the following alternative form for $\mathcal{R}$:

$$\mathcal{R} = \eta^u(z)\left[c_0^w\left(1 - Q(T)\right)\left\{q^{uC}(z) - q_0^w\right\} + c_0^I Q(T)\left\{q^{uC}(z) - q_0^I\right\}\right], \tag{36}$$

where c_0^w, q_0^w and c_0^I, q_0^I are auto conversion coefficients and threshold mixing ratios for water and ice respectively. [2] Using (32), (34) and (36) we compute λ (see appendix) and the vertical profile of q^{uC} and $\mathcal{R}$. If the computed λ is valid and if $\mathcal{R} \geq 0$, $(1 - Q(T))(q^{uC}(z) - q_0^w) \geq 0$ and $Q(T)((q^{uC}(z) - q_0^I) \geq 0$ at all levels, then we accept this solution. Otherwise, we take $q_0^w = q_0^I = 0$ as in MS99 and again solve for λ and q^{uC}. By doing this, we hope that at least for cloud types containing large amount of cloud condensate, we will be able to use nonzero critical mixing ratio. Of course, setting the critical mixing ratios to zero retrieves the solution of MS99.

4 Adaptation of the Cheng and Arakawa Downdraft

In this section we document the simplified version of the CA downdraft formulation (Cheng, 1989, CA97a, CA97b) applied to RASv2. Here the focus is on the RAS

[2] We have chosen $c_0^w = 0.001\text{s}^{-1}$, $q_0^w = 2.0 \times 10^{-5}$ kg/kg, $c_0^I = 0.4 \times 10^{-4}\text{s}^{-1}$, and $q_0^I = 2.0 \times 10^{-4}$ kg/kg in the results presented in this paper. It may be necessary to tune these parameters in a forecast model to obtain optimal results.

implementation and give only a brief summary of other details as they are documented in the above references. In CA the rain generated in the updraft may remain in the updraft or fall outside of the updraft. The rain that falls outside of the updraft can produce convective scale downdrafts through evaporation and frictional drag. Thus, the CA downdraft formulation has two major steps. The first step involves the determination of steady-state vertical profiles of the updraft vertical velocity, the rain flux within the updraft, and the rain flux that is falling into the environment. The second step involves the determination of the downdraft properties given the available rain flux and other properties of the updraft, such as its tilt.

4.1 Updraft Properties and Rain Flux

The CA downdraft scheme determines vertical profiles of the rain flux within the updraft and the rain flux available for the downdrafts by finding the stationary solution of the coupled rain-water budget and the vertical momentum equations for the updraft.

The stationary rain-water budget equation is written as (see Cheng 1989 for details)

$$\frac{\partial}{\partial z}\left[\frac{\eta^u}{w^u}\left(w^u - V_t^u \cos^2\theta\right)\right] + \frac{2f_2}{\pi a}\frac{\eta^u}{w^u} q_r^u V_t^u \sin\theta = \mathcal{R}, \tag{37}$$

where w^u is the vertical velocity, θ is the updraft's tilting angle measured from the vertical, a is an estimate of the average updraft radius, q_r^u is the rain water mixing ratio, and V_t^u is the average terminal velocity of the rain drops in the updraft. The first and second terms on the l.h.s. of this equation represent the vertical convergence of in-cloud rain flux and the outgoing rain flux per unit height from the side of the updraft per unit cloud-base mass flux. The term on the r.h.s. is the rate of rain water generation per unit cloud-base mass flux per unit height, as given by (36).

The stationary vertical momentum equation for the updraft is written as

$$\frac{\partial}{\partial z}\left(\eta^u w^u\right)^2 = 2(\eta^u)^2 \frac{B^u - g q_r^u}{f_1(1+\gamma^*)}, \tag{38}$$

where $\gamma^* = 0.5$ is the virtual mass coefficient [3] (Simpson and Wiggert, 1969; Cheng, 1989). The term on the l.h.s. of (38) is the vertical flux divergence of the updraft vertical momentum, while the r.h.s. represents the vertical momentum generation by buoyancy.

The parameters f_1 and f_2 in (38) and (37) are an attempt to account for the horizontal structure of updrafts. Following Cheng (1989), we have chosen $f_1 = 2.0$ and $f_2 = 1.5$. In CA97a and CA97b, f_1 and f_2 were set to unity. The terminal velocity V_t^u of the rain drops in the updraft is assumed to be given by the empirical formula:

$$V_t^u = 36.34\,(10^{-3}\rho^u q_r^u)^{0.1364}\,(\rho^u/\rho_0)^{-0.5}(\text{m s}^{-1}), \tag{39}$$

where ρ^u is the updraft air density [4] and ρ_0 is a reference air density taken as 1.2 kg m^{-3}.

For a given tilting angle θ, and using V_t^u from (39) and $\mathcal{R}$ from (36), the discrete versions of (37) and (38) can be solved iteratively following the method described in CA97a and CA97b. CA found two types of solutions for these equations: solutions for small tilting angle, which are unstable, and solutions for large tilting angle, which are stable. They showed that the solutions for large tilting angle do not show much dependence on tilting angle θ. They also pointed out that in the large tilting angle range the precise choice of θ is not very important, since the outgoing rain flux, which drives the downdraft, is more or less independent of θ. In their implementation, CA chose the smallest value of θ in this stable range, after solving the above equations for a number of tilting angles.

During our experimentation with these equations, we also found that the vertical distribution of updraft rain water, the vertical velocity, and the rain flux available for the downdraft are not too sensitive to the tilting angle. Therefore, for the sake of computational economy, we prescribe a sufficiently large tilting angle (so that the

[3] The virtual mass coefficient γ^* was introduced by Simpson and Wiggert (1969) to include the effect of acceleration of surrounding fluid.

[4] In our calculations, we have used the environmental air density instead of the updraft air density in (39). Since the density of the updraft air is slightly smaller than that of the environment, this approximation would decrease the terminal velocity by a few percent. Considering that (39) is empirical this assumption is not too extreme.

solution, if it exists, belongs to the stable range at least most of the time) for each cloud type and solve (37) and (38) once for each sounding and each cloud type. If the solution exists, we invoke the downdraft; otherwise, we assume that there is no downdraft associated with that cloud type. With this approach it is possible that we may miss some downdraft solutions for some cloud types. However, we make this compromise to avoid the otherwise prohibitively expensive computations involved in following CA's approach. At present θ is prescribed as a function of the pressure at the detrainment level, varying between a value of 35° for clouds detraining at 100 hPa and 15° for those detraining at 500 hPa. The updraft radius a is taken as $0.2/\lambda$ subject to an upper limit that again depends on the detrainment level. The upper limit of the radius is taken to vary between as 8 km for clouds detraining at 100 hPa and 1.0 km for those detraining at or below 500 hPa.

4.2 The Downdraft Model

Again, we follow the downdraft model of CA. For convenience, we will repeat the necessary equations. In these equations, as in CA97a and CA97b, we assume that z increases downward and that mass flux and vertical velocity are positive downward. Equations governing the conservation of mass, moist static energy, and moisture in the downdraft can be written as (superscript "d" denotes downdraft quantities)

$$\frac{d\eta^d}{dz} = \epsilon - \delta, \tag{40a}$$

$$\frac{d\eta^d h^d}{dz} = \epsilon h - \delta h^d, \tag{40b}$$

$$\frac{d\eta^d q^d}{dz} = \epsilon q - \delta q^d + E_r, \tag{40c}$$

where η^d is the downdraft mass flux normalized by the cloud-base mass flux of the updraft, M_B; ϵ, and δ are the normalized entrainment into and detrainment from the downdraft; h^d and q^d are the moist static energy and specific humidity of the downdraft air; and E_r is moisture source due to evaporation of falling rain, taken as

$$E_r = \sigma \frac{(1 - q^d/q^{*d})\, C\, (10^{-3}\rho^d q_r^d)^{0.525}}{5.4 \times 10^5 + 2.55 \times 10^6/(pq^{*d})}, \tag{41}$$

where σ is the fractional horizontal area covered by the downdraft per unit cloud-base mass flux of the updraft; q^{*d}, q_r^d, and ρ^d are the downdraft saturation specific humidity, rain water mixing ratio, and air density, respectively; p is the pressure in units of hPa; and C is a nondimensional ventilation coefficient, given by

$$C = 1.6 + 124.9\,(10^{-3}\rho^d q_r)^{0.2046}. \tag{42}$$

The vertical momentum equation, the rain-water budget equation, and the equation governing the vertical variation of σ for the downdraft as used by CA are:

$$\frac{d\eta^d w^d}{dz} = -\frac{\eta^d}{w^d}\frac{B^d - g q_r^d}{f_5(1+\gamma^*)} - \delta w^d, \tag{43}$$

$$\frac{dP^d}{dz} = \mathcal{R}_A - E_r, \tag{44}$$

and

$$\frac{\partial\sigma}{\partial z} = \frac{V_t^d}{w^d + V_t^d}\left(\frac{2}{\rho^u \pi a}\frac{\eta^u}{w^u}\sin\theta\right) - \frac{\sigma}{\rho^d}\frac{1}{w^d + V_t^d}\frac{\partial \rho^d w^d}{\partial z} - \sigma\frac{E_r}{P^d}, \tag{45}$$

where P^d is the rain-water flux in the downdraft given by,

$$P^d = \rho^d \sigma q_r^d\,(w^d + V_t^d), \tag{46}$$

and $\mathcal{R}_A$ is the normalized updraft rain water flux per unit height available for the downdraft, given by

$$\mathcal{R}_A = \left(\frac{2}{\pi a}\frac{\eta^u}{w^u} q_r^u V_t^u \sin\theta\right). \tag{47}$$

The downdraft air density at the level of downdraft origin is assumed to be identical to the environmental density. For all other levels, it is determined as a part of the solution to the set of downdraft equations given above. The terminal velocity, V_t^d, of falling precipitation in the downdraft is determined by the empirical formula (39) with q_r^d and ρ^d in place of q_r^u and ρ^u. In the first term of the r.h.s. of (45) the updraft density ρ^u is approximated by the environmental air density. The parameter f_5 in (43) relates to the horizontal structure of the downdraft; following Cheng (1989), we have chosen $f_5 = 2.5$. A detailed description of the iterative solution of the discrete forms of the above set of equations is available in CA97b. We have basically followed their procedure, but with some deviations, as discussed in the Appendix.

5 Modification of the Environment

5.1 Cumulus Effects on the Large-scale Budget

As in MS92, we divide the continuous spectrum of clouds into subensembles of finite $\Delta\lambda_i$. Thus, the rate of change of environmental temperature, specific humidity, liquid water mixing ratio, and ice water mixing ratio due to the i^{th} cloud ensemble with entrainment parameter between λ_i and $\lambda_i + \Delta\lambda_i$ can be written as

$$\left(\frac{\partial T}{\partial t}\right)_c = \frac{M_B(\lambda_i)\Delta\lambda_i}{c_p}\,\Gamma_s, \tag{48}$$

$$\left(\frac{\partial q}{\partial t}\right)_c = \frac{M_B(\lambda_i)\Delta\lambda_i}{L_c}\,[\Gamma_h - \Gamma_s + L_f\Gamma_I], \tag{49}$$

$$\left(\frac{\partial q^L}{\partial t}\right)_c = \frac{M_B(\lambda_i)\Delta\lambda_i}{c_p}\,\Gamma_L, \tag{50}$$

and

$$\left(\frac{\partial q^I}{\partial t}\right)_c = \frac{M_B(\lambda_i)\Delta\lambda_i}{c_p}\,\Gamma_I, \tag{51}$$

where Γ_s, Γ_h, Γ_L and Γ_I are the convection induced rates of change of environmental dry static energy s, moist static energy h, liquid water mixing ratio q^L, and ice water mixing ratio q^I per unit cloud-base mass flux $M_B(\lambda_i)\Delta\lambda_i$.

In evaluating Γ_s and Γ_h, we include contributions from both the updraft and downdraft associated with each subensemble. Thus,

$$\Gamma_s = g\left[\delta^u(s^u - s) - \eta^u\frac{\partial s}{\partial p} + \frac{\partial\{\eta^d(s^d - s)\}}{\partial p} - \beta\{L_c q^{uT} + L_f q^{uI}\}\right] \tag{52}$$

and

$$\Gamma_h = g\left[\delta^u(h^u - h) - \eta^u\frac{\partial h}{\partial p} + \frac{\partial\{\eta^d(h^d - h)\}}{\partial p}\right], \tag{53}$$

where δ^u is the detrainment per unit pressure interval in the updraft. In our current formulation, we allow detrainment of condensate from the updraft only at the cloud top. In evaluating Γ_L and Γ_I, we include only contributions from the updraft:

$$\Gamma_L = g\left[\delta^u(\{1-\beta\}q^{uL} - q^L) - \eta^u\frac{\partial q^L}{\partial p}\right] \tag{54}$$

and

$$\Gamma_I = g\left[\delta^u(\{1-\beta\}q^{uI} - q^I) - \eta^u\frac{\partial q^I}{\partial p}\right]. \tag{55}$$

Here β is the fraction of the detrained cloud condensate that is assumed to evaporate immediately in the detraining layer. If the environment does not contain liquid water or ice, then (54) and (55) have a contribution only from detrainment. Discrete forms of these equations are given in the Appendix.

It should be noted that in (52)-(55) we do not allow for phase changes of cloud condensate during detrainment. Depending on the application and on the parameterization of microphysical and precipitation processes in other parts of the model, one may wish to modify this assumption. In the present application, we are assuming that the detrained condensate is available as a source term for the prediction of condensate in the environment.

5.2 The Mass-flux Kernel and Cloud Base Mass Flux

The mass-flux kernel is defined as the rate of change of cloud work function per unit cloud-base mass flux. In MS92 the mass-flux kernel was determined analytically by differentiating the expression for the cloud work function. However, it is difficult to do so with the cloud work function as defined in (30). Therefore, we calculate the mass-flux kernel numerically by following the approach used in the standard implementation of AS as in Lord et al. (1982). In this approach we first calculate the cloud work function of a subensemble; we then use a small "test" cloud-base mass flux and modify the sounding using (48) and (49). Using this modified sounding, we recalculate the cloud work function. The mass-flux kernel $\mathcal{K}_i$ is then estimated as the change in the cloud work function divided by the test mass flux.

Once the mass-flux kernel is known, we can compute the cloud-base mass flux necessary to completely balance the large-scale effects on the cloud work function (see MS92 and Lord et al., 1982, for further details). The final adjustment of the large-scale environment is then made using a fraction α_{λ_i} of the mass flux needed to fully adjust a single cloud type (see MS92). Thus, both the updraft and downdraft associated with a subensemble modify the environment when that subensemble is invoked and thus influence both updraft and downdraft properties of all subensembles invoked subsequently.

5.3 Evaporation of Falling Precipitation

The precipitation generated in the updraft eventually falls into the environment or the subcloud layer. Such falling precipitation in an unsaturated environment undergoes evaporation, often producing downdrafts. In the original RAS, evaporation of falling precipitation was not included. Moorthi (2000) included a simple scheme based on the formulation of Sud and Molod (1988) in the original RAS. In the version of RAS presented here, evaporation in the environment and the associated downdraft are determined using the CA approach. However, we do encounter situations in which a downdraft does not form. Also, we may not perform downdraft calculations for shallow cloud types to save computer time. Furthermore, we allow the option of starting the downdraft from a level below the top of the updraft. For all of these situations, we compute the evaporation of falling precipitation following the Sud and Molod (1988) approach as described in Moorthi (2000).

When no downdraft exists or when there is no solution for the rain-water budget equation (37), we assume that all rain falls into the environment at the level where it is generated, as in the original AS. This rain profile is used in the evaporation calculation. If a solution to the rain flux equation (37) exists, but no downdraft solution exists, then the rain flux profile is used as the rain available for evaporation. If the downdraft calculation is done from a level below the updraft top, then any rain flux above that level is also available for evaporation outside of downdraft. Also, if the downdraft stops before reaching the ground due to loss of buoyancy, then the

rain falling through the bottom of the downdraft undergoes evaporation. Rain falling from the bottom of the updraft may also contribute to evaporation in the subcloud layer. Finally, there can be situations when we start the downdraft calculation from a layer (*e.g.* cloud top), but downdraft does not start (*i.e.* no solution to downdraft equations) in this layer. For these situations, we simply let the rain flux drop to the layer below until the downdraft starting level is reached.

6 Application Strategy

Until now we have documented the methodology for calculating the modification of the environmental sounding due to a single cloud type. As stated before, in RAS we invoke one cloud type at time, letting each cloud type modify the environment partially. Thus over a reasonable time period, the destabilization due to the large-scale forcing and the stabilization due to the cumulus convection will be in quasi-equilibrium.

We generally represent a cloud type by the level of detrainment. In a model with K layers, there can be, at most, $K-1$ cloud types with k^{th} cloud type representing an ensemble of clouds detraining between pressure levels $p_{k+\frac{1}{2}}$ and $p_{k-\frac{1}{2}}$. A full spectrum would include all clouds detraining between the model top and the level of free convection. Then for a reasonably good representation of the full spectrum, we need to be able invoke all possible cloud types within a reasonable period.

When the number of model levels become large, the number of possible cloud types also becomes large. This implies that the cloud spectrum is divided into finer subensembles, and covering the full spectrum requires invoking more cloud types with a smaller relaxation parameter. This implies that the cost scales like the number of levels squared. We did not worry about this in the original RASv1 because it was fairly inexpensive and was being used in relatively coarse models. RASv2, however, is computationally intensive and invoking all cloud types can be prohibitively expensive. To mitigaite this we currently invoke all shallow cloud types below $\frac{p}{p_s} < 0.76$ and call a set of random cloud types where $0.76 < \frac{p}{p_s} < 0.05$, where p is the cloud top pressure

and p_s is the surface pressure. We currently specify a fixed number of random clouds per hour of forecast time so that the number of random clouds are more or less invarient with respect to model time step (however, at lest one random cloud type is invoked every physics time step), thus keeping RASv2 computationally competitive.

Another possible strategy, when the vertical resolution of the model is high, is to view the cloud spectrum as a set of discrete $\Delta\lambda$'s. We can divide the pressure domain that represents the full spectrum of detrainment levels into a reasonable number of cloud types with a fairly thick detrainment layer of ($\approx$ 50 or 100 hPa). Then, using these pressure thickness as a guide, we can strap one or more layers of a higher vertical resolution model to come up with a modified cloud spectrum with somewhat thicker detrainment layers. Invoking several of these cloud types every time-step can cover the full spectrum in a short time. Within each of the strapped layers the modification of the environment due to a given cloud type can be assumed to be the same. This option is not availeable in RASv2 implementation available under ccpp-physics at this time. However, this strategy was used in the results presented in the semi-prognostic and single column results pesented below.

7 Semi-Prognostic Evaluation

As demonstrated by Lord (1978, 1982), Krishnamurti et. al., (1980), Kao and Ogura (1987), and others, the semi-prognostic test is a very useful tool in the development and evaluation of a cumulus parameterization scheme. RASv1 was tested by MS92 using both the semi-prognostic and the single column prognostic approach. MS92 found that while the obtained cumulus heating profile was reasonable, the cumulus drying was excessive compared to the observed estimate. This result is consistent with those for the original implementation, as shown in Lord (1978). Moorthi (2000) showed that inclusion of evaporation of falling convective rain does not completely reduce the excessive drying. We have tested ia version of RASv2 described herein with the semi-prognostic approach also and the results are reported in this section.

For this purpose, we use the same GATE phase III data employed by MS92. The

daily mean radiation data are from Cox and Griffith (1978) and all other data are as analyzed by Thompson et al., (1979). Surface evaporation and sensible heat flux, and the turbulent fluxes in the boundary layer are estimated using the boundary layer formulation of the National Centers for the Environmental Prediction (NCEP) Medium Range Forecast (MRF) model (Hong and Pan, 1996). We use 40 layers of equal pressure depth in the vertical between the surface and the top of the atmosphere. The lowest three model layers are taken as the subcloud layer for RASv1. In RASv2, the cloud base and the subcloud layer are determined within the algorithm and can vary in time and space.

In the semi-prognostic test performed in MS99 two possible choices for the sub-cloud layer top (level $K - \frac{1}{2}$) moist static energy and specific humidity were tested. It was found that the choice of mean subcloud layer value produced relatively poor result compared to the choice of average value between the sub-cloud layer and the layer above. Therefore, in the results presented in this section, we only use the latter option. With this choice, the cumulus induced subsidence in the environment can directly modify the subcloud layer properties.

Figure 2a,b shows the time-averaged convective heating and moistening as a function of height. In these figures, thick solid lines (RV1) correspond to RASv1, as currently used in the NCEP Seasonal Forecast Model, with evaporation of falling convective precipitation. It also includes evaporation of part of the rain at the detrainment level when the cloud top is below 400 hPa. The thin solid lines (RV2LND) are for the RASv2 with the linear entrainment relation and no downdraft. This version of RAS also includes evaporation of falling precipitation as used in RASv1. We also allow the detrained condensate at the cloud top to partially evaporate within the detrainment layer and partially evaporate in the environment as it falls, using a scheme similar to that used for evaporation of falling large-scale precipitation in the NCEP operational global model. The long dashed lines (RV2QND) are for RASv2 with the quadratic entrainment relation and no downdraft. The dotted lines (RV2QDT) are for RASv2 with the quadratic entrainment relation and a downdraft starting from the detrainment level. The short dashed lines (RV2QDM) are for the case when the downdraft is allowed to start from the level of minimum moist static energy. The thick dash-dot

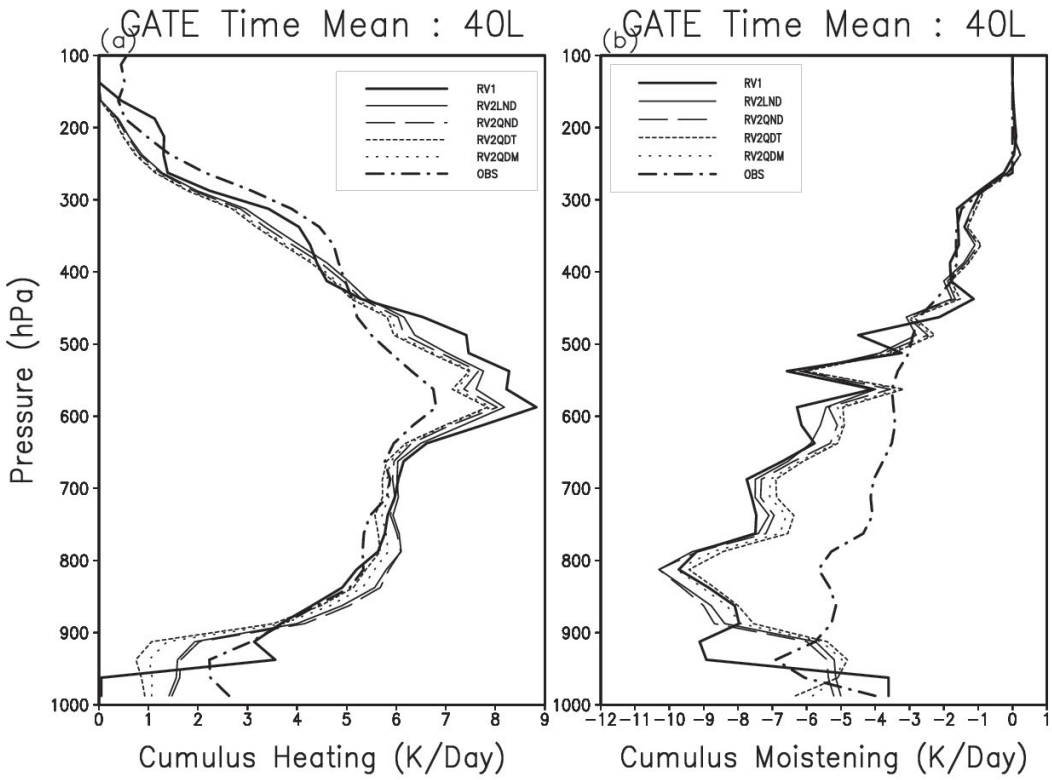

Figure 2: The time-averaged convective (a) heating (K/day) and (b) moistening (K/day) as a function of height obtained in the semi-prognostic test using the GATE Phase III data. The moist static energy and moisture at the top of the subcloud layer is taken with the value of moist static energy and specific humidity at the subcloud layer top are taken as a mean of the corresponding values within the subcloud layer and the layer above. A value of $\alpha_i = 0.3$ (the relaxation parameter) is used for all cloud types. The thick dash-dot lines represent the observed estimates of $(Q_1 - Q_R)/c_p$ and $-Q_2/c_p$. The thick solid lines are for the convective heating and moistening rates for the RASv1. The thin solid lines are for RASv2 with linear entrainment case and no downdraft. The long dashed lines is for quadratic entrainment case without downdraft. The short dashed lines are for the case of quadratic entrainment with downdraft. The dotted lines are also for the same case but with the downdraft starting from the level of minimum moist static energy.

lines represent observed estimate of cumulus heating and moistening. They are obtained from the apparent heat source, Q_1, and moisture sink, Q_2 (Yanai et al., 1973), in the GATE data set, with daily mean radiation data from Cox and Griffith (1978), and surface fluxes and their vertical distribution estimated using NCEP boundary layer formulation. It should be pointed out that the model generated heating and moistening balance exactly when vertically integrated. However, this is not true for the observed estimate and therefore, one should be cautious in comparing the two. It is probably more accurate to assume that the temperature measurement is more reliable than the humidity measurement. Although there is some uncertainty in the radiation data, it is likely that the observed estimate of cumulus drying is too small.

From Fig. 2 we infer that RASv1 produces higher heating at virtually all levels below 400 hPa than the observed estimate. Cumulus drying is also larger than the observed estimate at almost all levels. RASv2 with linear entrainment produces very similar results with slightly more (less) heating at lower (upper) levels and slightly more (less) drying at lower (upper) levels. Inclusion of the quadratic entrainment relation changes the results only slightly. When the downdraft is included, the heating profile is closest to the observed profile below 400 hPa and cooler than observed above that level. Cumulus drying is clearly the lowest with the downdraft included. The profiles obtained when the downdraft is started from the level of minimum moist static energy is slightly inferior. It is apparent that even with downdraft there is significant difference between observed estimate and predicted cumulus moistening. It should be remarked that the vertically integrated cumulus heating is very close to the observed estimate. Since the predicted heating exactly balances the predicted drying, the large difference we see in Fig. 2 between the observed estimate and predicted drying can only be interpreted as a consequence of uncertainty in the observed estimates. From these results, we can conclude that the new RAS produces acceptable results. However, these semi-prognostic tests are insufficient to show whether RASv2 is significantly superior over RASv1.

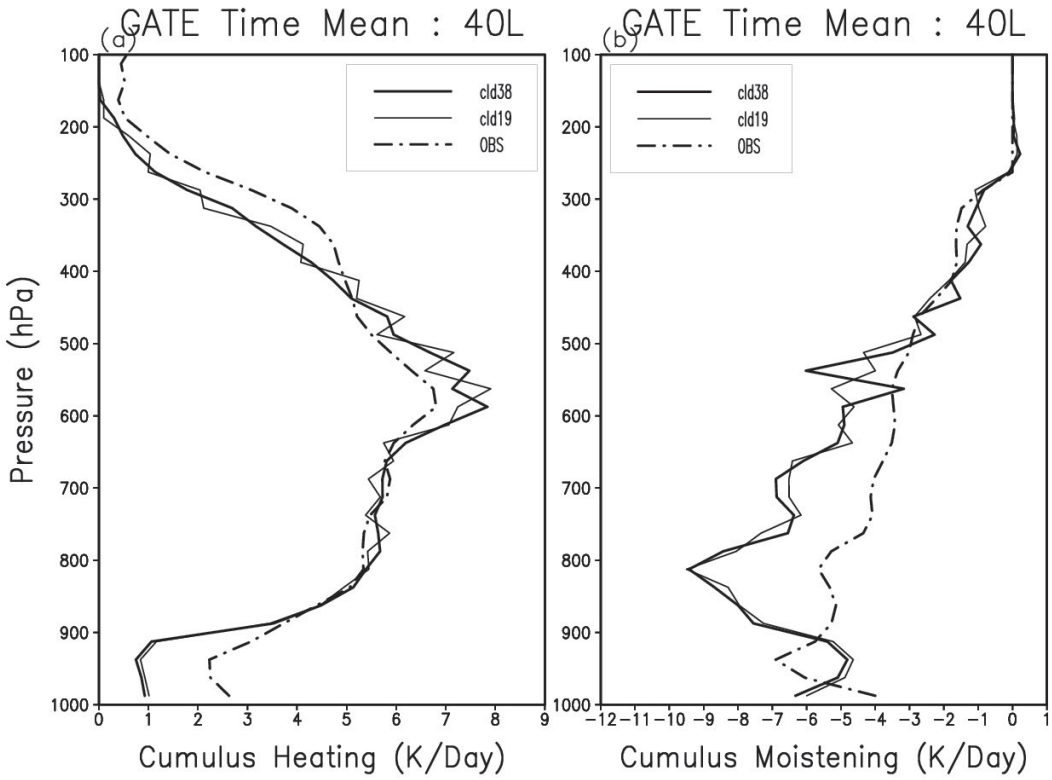

Figure 3: The time-averaged convective (a) heating (K/day) and (b) moistening (K/day) as a function of height obtained in the semi-prognostic test with 40 equally spaced vertical levels. The thick dash-dot lines represent the observed estimates of $(Q_1 - Q_R)/c_p$ and $-Q_2/c_p$. The thick solid lines are for the convective heating and moistening rates when 39 cloud types are allowed. The thin solid lines are for the case with 19 cloud types having two strapped model layers as detrainment layers. A value of $\alpha_i = 0.3$ is used for both cases.

8 Single Column Model (SCM) Results

In this section we present results from the application of RASv1 and RASv2 to a version of the Natinal Centers for Environmental Prediction (NCEP) single column model (SCM) for the GATE period. Most of the physical parameterizations in the NCEP SCM used here are identical to the NCEP operational medium range forecast (MRF) model of 1999/2000, with some minor differences. One difference is that we use an earlier version of large-scale precipitation scheme instead of the MRF version which also includes convective adjustment. We have modified this large-scale precipitation scheme to handle the detrained cloud condensate by treating it the same way as large-scale condensation. To be fair to RASv1, we have chosen not to use prognostic cloud condensate in the version of SCM used here. Other physical parameterizations included in the SCM are surface and boundary layer processes (Hong and Pan 1996), shallow convection scheme, and radiation. The convection scheme of the operational MRF (Pan and Wu, 1995) is replaced by either RASv1 or RASv2.

The SCM is integrated from 30 August, 1974, 00 UTC to 18 Septmember, 1974, 00Z. The adiabatic tendencies of temperature and specific humidity at every time step is obtained through linear interpolation from three hourly observed tendencies from the GATE data. Both shortwave and longwave radiation are calculated every hour. However, the radiation increments are applied every time-step (see Hou et al. 1996, for radiation details), which is taken as 300s. To be consistent with the MRF model, the SCM also uses a leap-frog scheme with an Asselin time filter. Since adiabatic tendencies for the velocity components are not available, gravity-wave drag and vertical diffusion in the physics package is not used and the the total tendency of velocity components calculated by finite differencing the observed velocity components is used in forcing the model velocity components.

A 28 layer version of the SCM is used in this study, the 28 layers corresponding to those used in a version of the MRF model. For RASv1 experiment all possible cloud types are invoked. Using the application strategy described in the previous section, 15 cloud types are invoked for the RASv2 experiment. A relaxation parameter of α=0.3 and rain reevaporation parameter of 5 (R_k in Moorthi, 2000) is used for both

experiments.

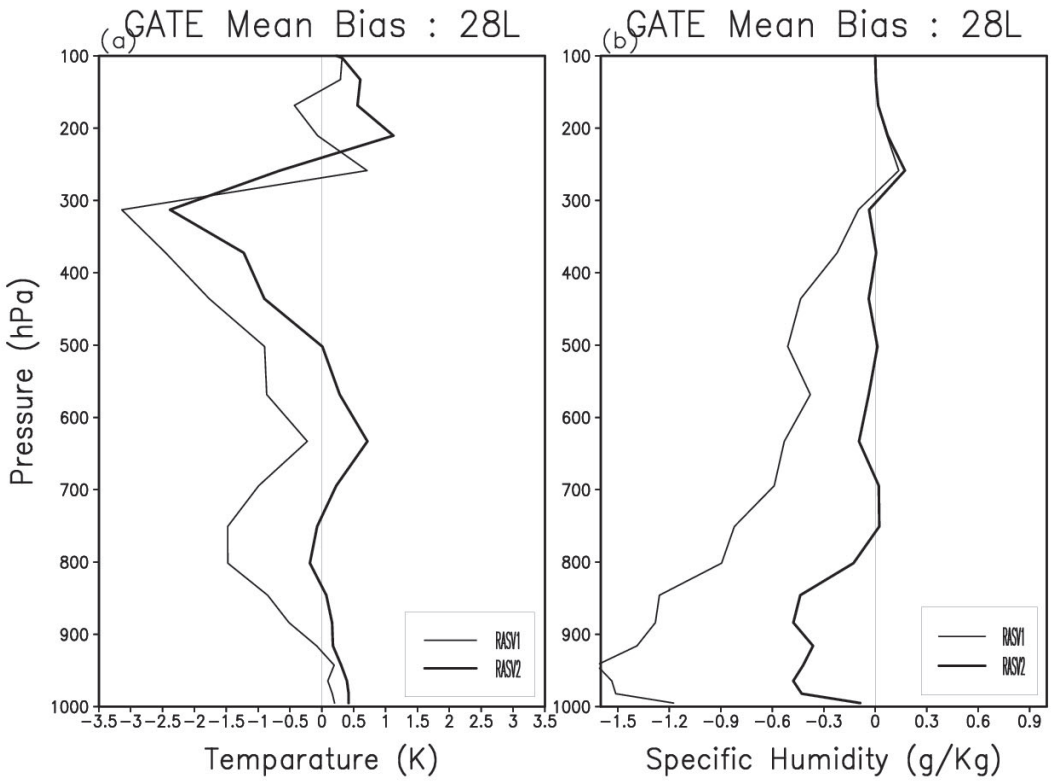

Figure 4: Predicted temperature and specific humidity bias for RASv1 (thin line) and RASv2 (thick line)

Figures 4a,b show the time mean difference between the observed and predicted bias of temperature and specific humidity for RASv1 (thin solid line) and for RASv2 (thick solid line). Corresponding root mean square (rms) errors are shown in Figs. 5a,b. RASv2 is clearly warmer than the RASv1 and the former seems to have less bias except near the bottom. The moisture bias is generally a dry bias, but RASv2 has much smaller bias compared to that for RASv1. The rms errors are also smaller for RAS V2 for both temperature and moisture. Of course, not all the physics of the model is perfect, so we can only conclude here that RASv2 performs as good as or better than RASv1.

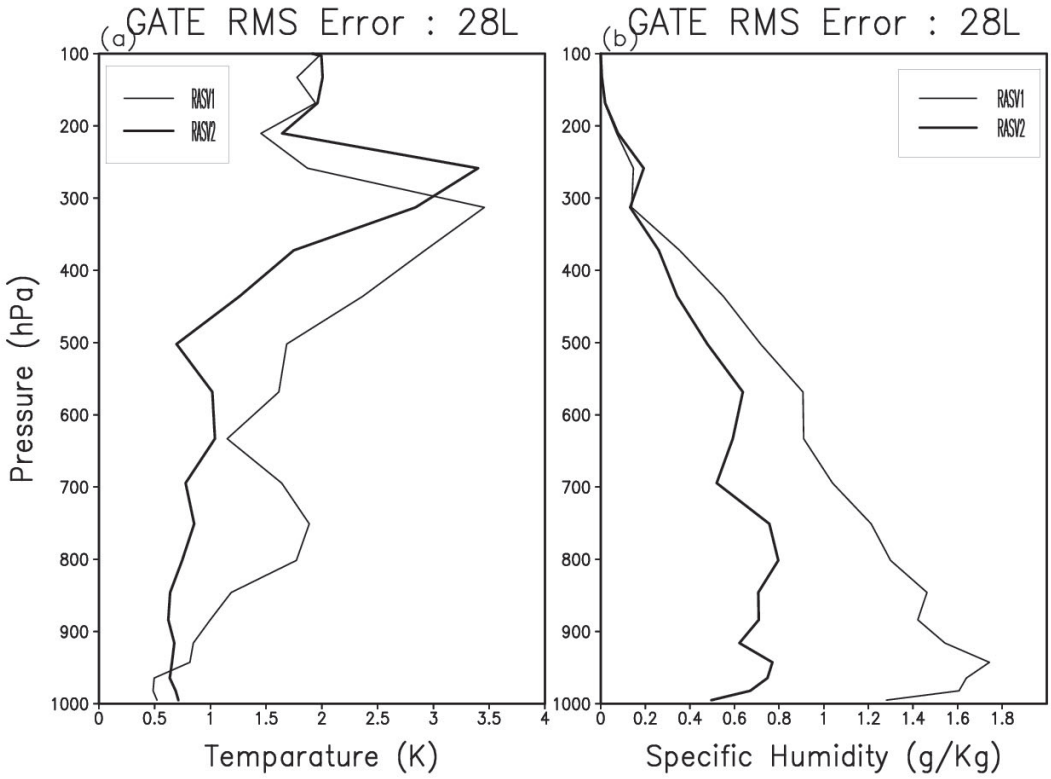

Figure 5: Same as in 4 but for rms erros.

Figures 6a,b show the time mean Q_1 and Q_2 for the RASv1 (thin solid line) and RASv2 (thick solid line). Observed estimate is shown as thick dashed line. The rms errors for Q_1 and Q_2 are shown in figures 7. From these figures, it appears that RASv2 is somewhat better than RASv1 with smaller rms errors and closer to observed estimate.

In Figs. 8a,b,c we show the observed estimate (panel a) of the apparent heat source Q_1 and as predicted by SCM for RASv1 (panel b), for RASv2 (panel c). Note that the predicted Q_1 is the sum of heating due to convection, grid-scale condensation, shallow convection, vertical diffusion, and radiation. Corresponding figures for the apparent moisture sink Q_2 are shown in Figs. 9a,b,c. These figures show that both versions of

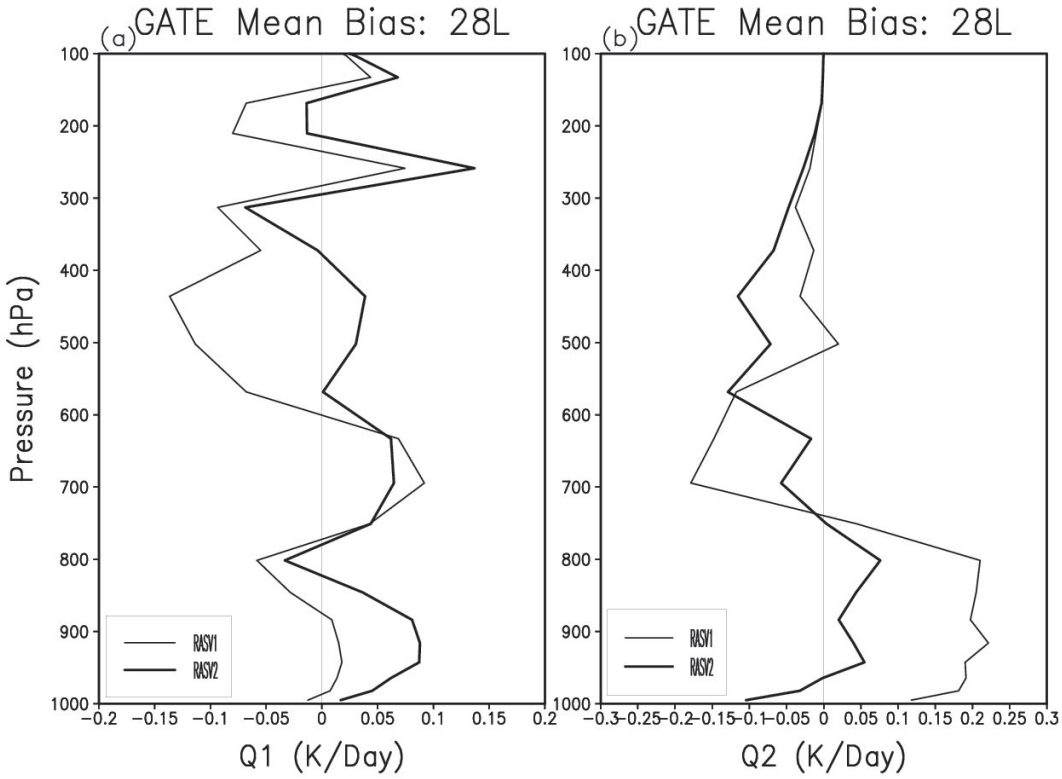

Figure 6: Same as in 4 but for Q_1 and Q_2

RAS capture most of the observed convective episodes and that the RASv2 may be slightly superior to RASv1.

9 Recent updates

In this section we document some of the recent updates within RASv2. It includes a simple treatmentis for vertical advection and scale-awareness.

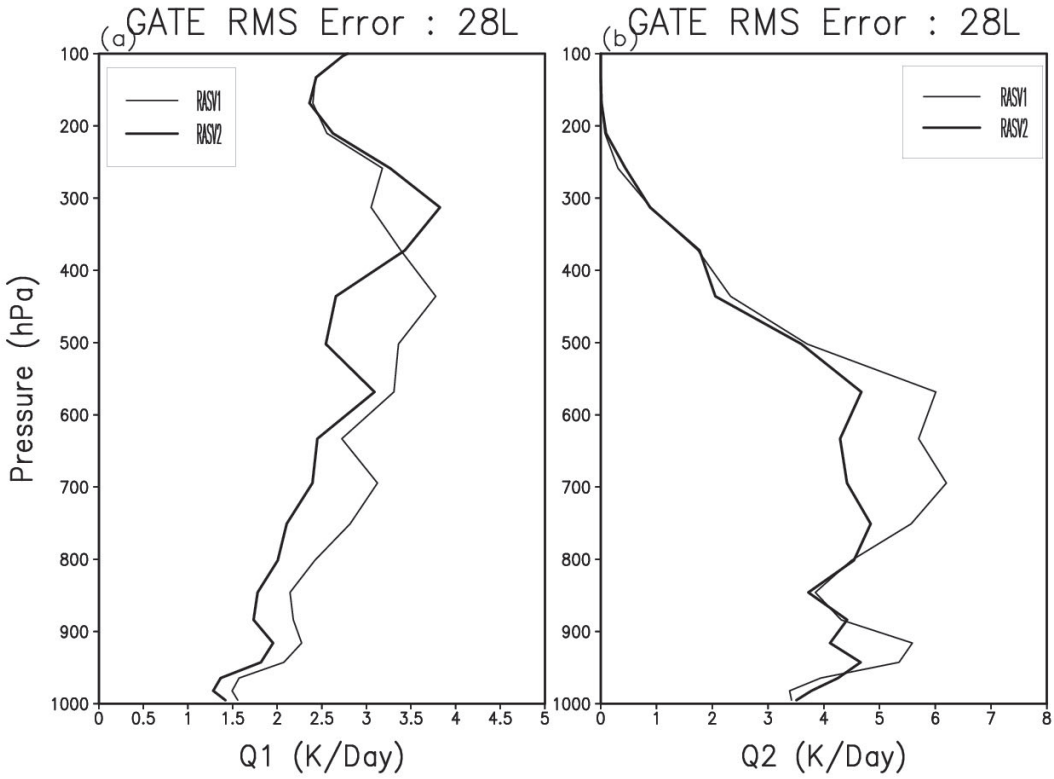

Figure 7: Same as in 5 but for Q_1 and Q_2.

9.1 Quasi-positive definite vertical advection of cloud condensates and tracers in the environment

It was found that using the centered differencing for the vertical advection by the environmental subsidence (see the vertical discretization in the appendix) produce negative values for all tracers, including cloud condensates. Using an upstream scheme would eliminate these negative values, but is too smoothing. In the current verison of RASv2, we have added an option to use a total variance diminishing (TVD) scheme for advection by subsidence. We achieve this by defining the values of the advected parameter at the interface levels folowing TVD approach (see Thuburn, 1996, eq.

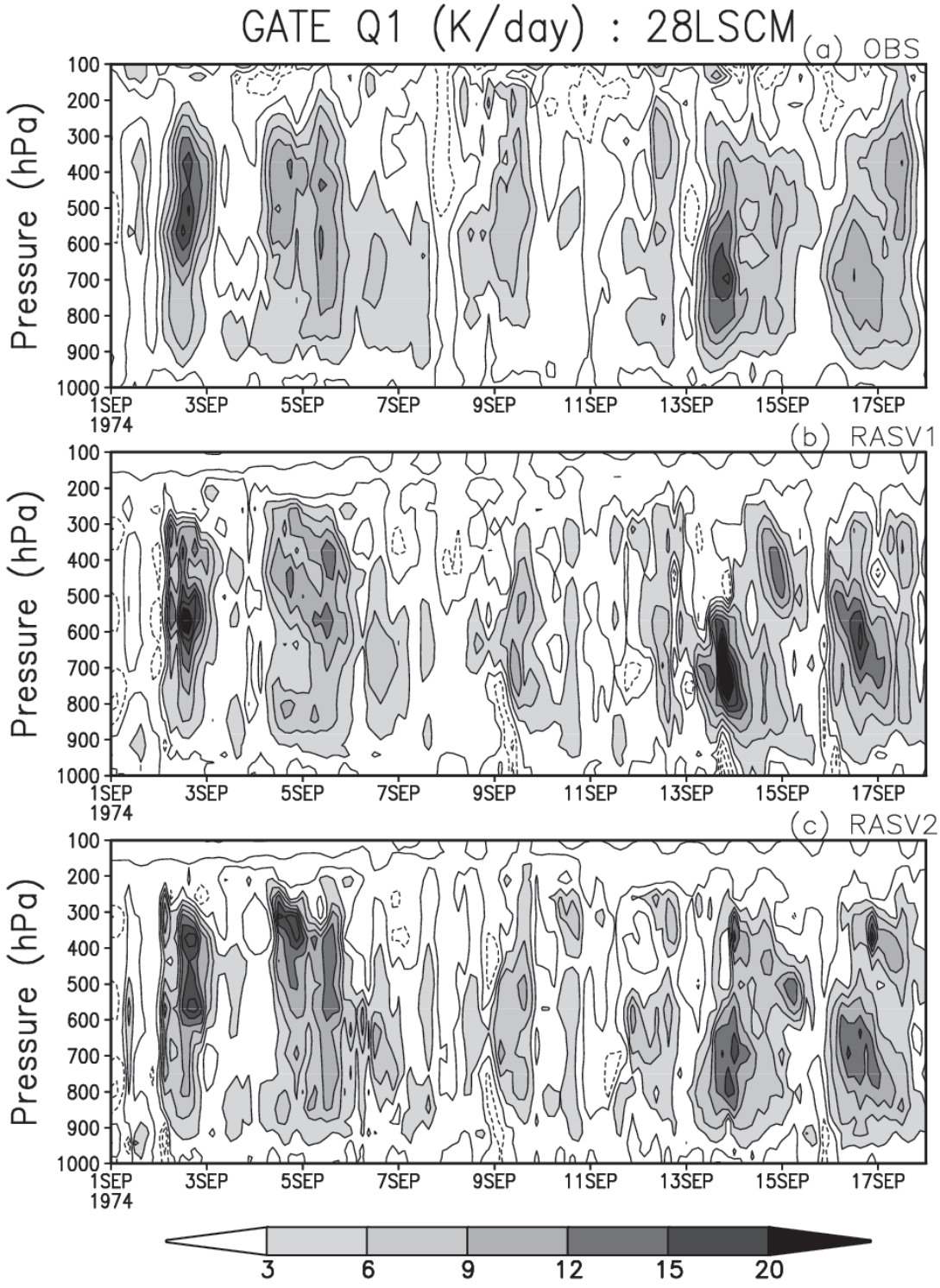

Figure 8: Time evolution of Q_1 (a) observed, (b) SCM predicted with RASv1 and (c) with RASv2. Units K/day

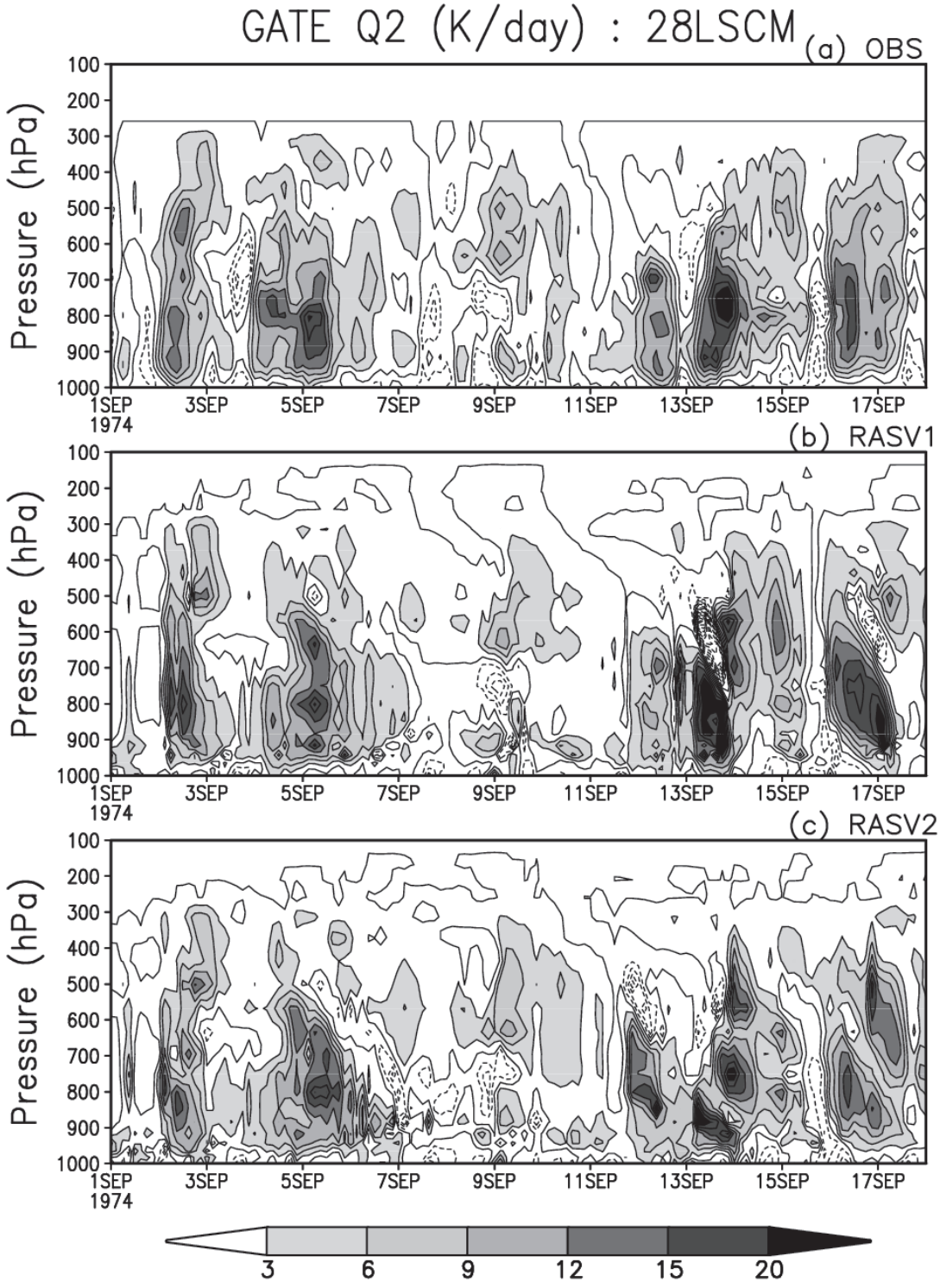

Figure 9: Same as in fig. 8a,b,c. but for Q_2

(13)). To save computation time the flux limter terms are computed once per time step.

9.2 A simple implementation of scale-awareness

Following Arakawa and Wu (2013), to achieve scale-awareness, we have added an option to modifify the cloud base mass flux by scaling it with the factor $(1 - \sigma)^2$ where the updraft area fraction σ is estimated from the entrainment parameter λ using the relation

$\sigma = 0.2/max(\lambda, 1.0^{-5})$. As the updraft area fraction approaches one, the contributions from convective parameterization approaches zero.

10 Some results from application of RASv2 to coupled UFS

Over the last two decades, we have applied RASv2 to various versions of the NCEP Global Spectral Model with application strategy presented previously and the results were very promising. RASv2 was operational for many years in the NCEP NEMS-GOCART Aerosol Component (NGAC) model until NGAC model was recently replaced by FV3 based GEFS-GOCART model.

The current version of RASv2 is available under ccpp-physics package (see $https://dtcenter.org/community-code/common-community-physics-package-ccpp$). It has also been tested in various coupled/uncoupled NOAA Unified Forecast System (UFS). Details on the NOAA (UFS), which is a community-based, coupled, comprehensive Earth modeling system, are available at $https://ufscommunity.org$ and $https://ufscommunity.org/wp-content/uploads/2019/10/201903xx\ UFS\ Overview.pdf$.

Here we will present some results from experiments with application of RASv2 in coupled UFS in which FV3 based atmosphereic model is coupled to MOM6 ocean model, CICE6 sea-ice model, NoahMP land model, and CMEPS mediator. Details of the

ocean, ice and land models and the mediator used here are available in Stefanova et al., (2022). In additon to RASv2 for convection, we also use Simplified Higher Order Closure (SHOC) representation of bounbdary layer and shallow convection (Bogenschutz and Krueger, 2013) and Morrison and Gettelman version 3 (MG3 - Gettleman et al., 2019) microphysics. In this implementatiuon the cloud fraction is unified across SHOC, MG3 and radiation. Some results from this coupled UFS at a cubed sphere resolutions (atmosphere) of C384, C768, C1152 and C3072, all with 127 vertical layers, are presented below. Some additional results from a seasonal cycle run with an earlier version of coupled UFS with NEMS mediator, CICE5 ice model, and Noah land model with 64 vertical layers and $C384$ and $C768$ horizontal resolutions for the atmosphere are available at $https://dtcenter.org/sites/default/files/events/2020/1-moorthi-shrinivas-model-dynamics-physics-air-quality-moorthi-shrinivas.pdf$

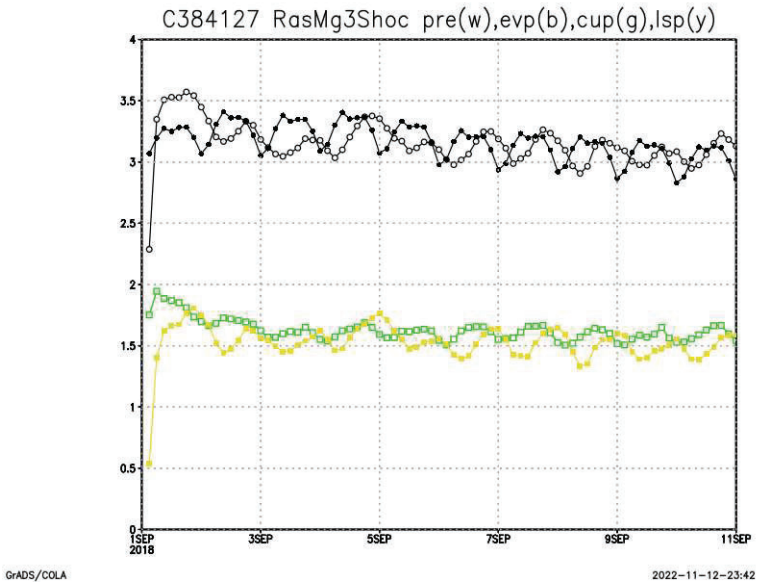

Figure 10: Time evolution of global mean precipitation (white circle), evaporation(black circle), convective precipitation (green circle) and resolved-scale precipitation (yellow circle) from $C384L127$ coupled UFS

In Figs. 10, 11, 12, and 13 we show global mean precipitation, evaporation, convective precipitation generated by RASv2 and resolved-scale precipitation generated by MG3

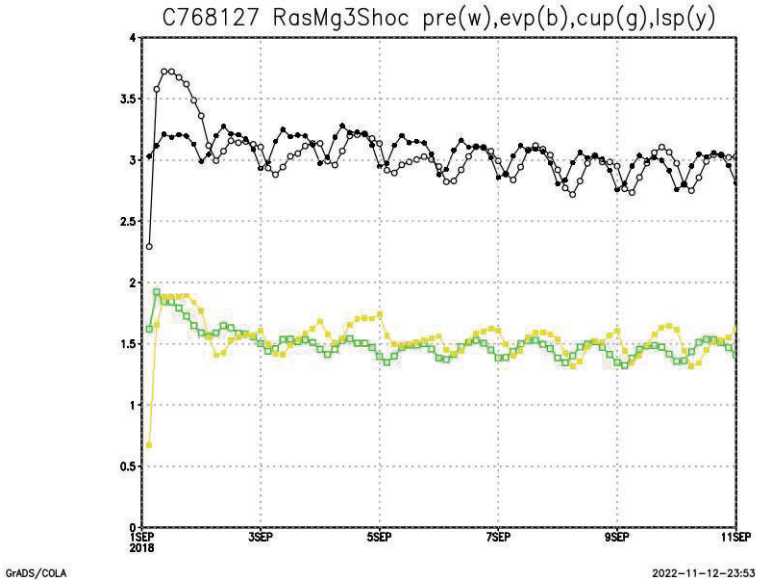

Figure 11: Same as in fig. 10 but for $C768$

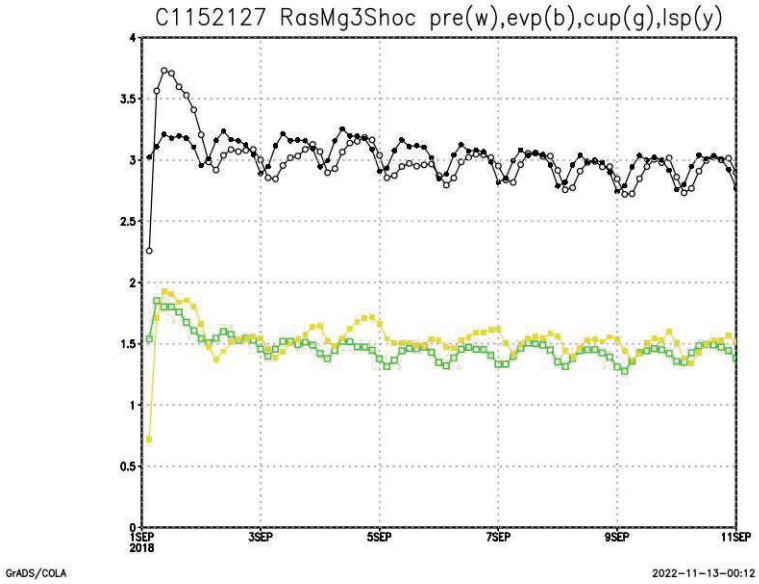

Figure 12: Same as in fig. 10 but for $C1152$

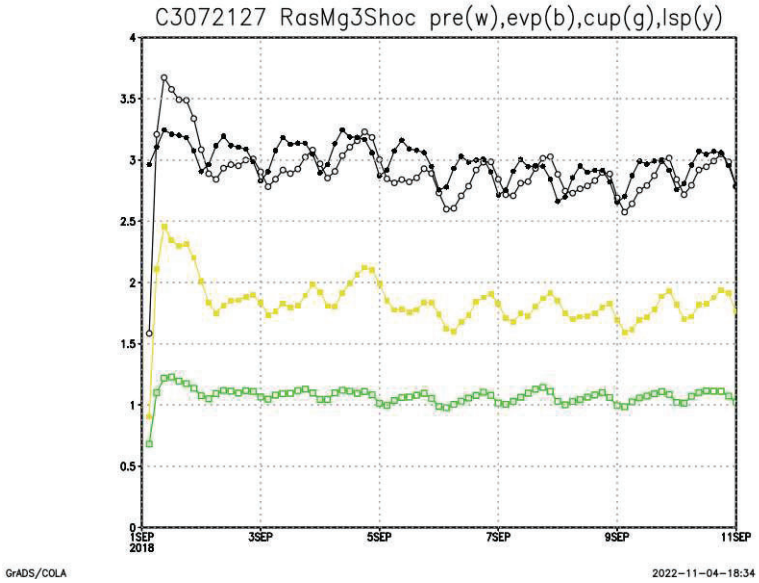

Figure 13: Same as in fig. 10 but for $C3072$

microphysics for atmospheric model resolutions of C384, C768, C1152 and C3072 repectively. Note that both evaporation and total precipitation are in good balance with each other at all four resolutions. The parameterized convective precipitation decreases and the resolved precipitation increases as the horiuzontal resolution is increased; however, the decrease of convective precipitation is not so dramatic for the resolution change from C384 to C1152. Nevertheless, at C3072 (3km horizontal grid resolution) the grid-scale precipitation dominates, but the convective precipitation is still not inegligible which indicates that comvective parameterization is important even at 3km horizontal resolution.

11 Summary

In this document we have presented an advanced version of the Relaxed Arakawa-Schubert convection parameterization. This version of RAS includes several important improvements over the original RAS. The cloud model now includes the virtual effects of moisture on buoyancy. It also includes condensate loading and takes into

account the production of precipitation as the updraft ascends. Quadratic entrainment is an option that is included with minimal additional complexity. A crude representation of ice phase for the condensate is also included. Detrainment at the cloud top provides a source of cloud condensate for models having cloud condensate as a prognostic variable.

Following Cheng and Arakawa (1997a,b), we have also incorporated a simplified version of their evaporatively driven downdraft into this version of RAS. For computational reasons, we have chosen to fix the vertical tilt of the updraft for a given cloud type. Even so, the scheme is quite expensive. For further economy, we have provided an option in the code to start the downdraft calculation from any level of the model at or below the detrainment layer. Since RAS invokes one cloud type at a time, one can also economize by invoking downdrafts only for deep cloud types.

A scheme for evaporation of falling precipitation is also included, in addition to the evaporation within the downdraft. This is necessary to account for evaporation in the absence of the downdraft.

We have presented some results from semi-prognostic tests of RASv2 with GATE data. Results showed that the performance of RASv2 is similar to that of the original RASv1 when the downdrafts are not included. It produces reasonably good (slightly larger) heating but excessive drying at lower levels. Inclusion of downdrafts reduces this low-level drying.

We also presented results from the NCEP SCM with both RASv1 ans RASv2. The SCM results further demonstrate that RASv2 performs as good as or better than RASv1.

Over the years RASv2 has been incorporated into various versions of NCEP spectral/semi-Lagrangian GFS. Recently it is also available via the common community physics package maintained by NCAR/DTC. It has also been tested in various coupled/uncoupled UFS settings. Here we presented some recent results from coupled UFS using CMEPS mediator and ccpp based physics with RASv2 coupled with SHOC for boundary layer/shallow convection and MG3 for microphysics.

An advantage of RASv2 over the RASv1 is in providing a good estimate of the detrained cloud condensate. It also provides precipitation at all levels. This is an improvement over the original RAS in which the precipitation occurs only at the cloud top. In the earlier version we arbitrarily used a fraction of this precipitation at the cloud top as detrained cloud condensate. RASv2 removes the need for this arbitrariness. Also, with the precipitation falling from different heights, its evaporation in the environment can be expected to be more realistic compared to the way in which it is treated in RASv1 (Moorthi, 2000).

Acknowledgements

I thank Dr. Max Suarez of GSFC (Retired) for his contributions to the development of RAS, Late Professor A. Arakawa of UCLA and Dr. M.-D. Cheng of Central Weather Bureau, Taiwan for their help in understanding their downdraft formulation. I also thank Dr. S. Lord (EMC/NCEP, retired) for providing encouragement during major development stage of RASv2. I also thank Ms Mary Hart for her tireless help in getting this document published and thank Drs Fanglin Yang and Brian Gross for approving the publication.

Appendix

Vertically Discrete Formulation

We now consider the vertically discrete system. In order to resolve the planetary boundary layer, most modern models have many layers in the lower troposphere. Therefore, in our present discrete formulation, we allow for more than one layer below the cloud base. Thus, we divide the vertical domain into $K + M - 1$ layers and index the variables vertically from top to bottom. Layer 1 represents the top layer of the atmosphere, while layer K represents the first layer in the subcloud layer just below the cloud base and M is the total number of subcloud layers ($M \geq 1$). Any

layer k is bounded by edge levels $k - \frac{1}{2}$ and $k + \frac{1}{2}$. The environmental temperature T, specific humidity q, and any condensate are assumed to be defined at the layers.

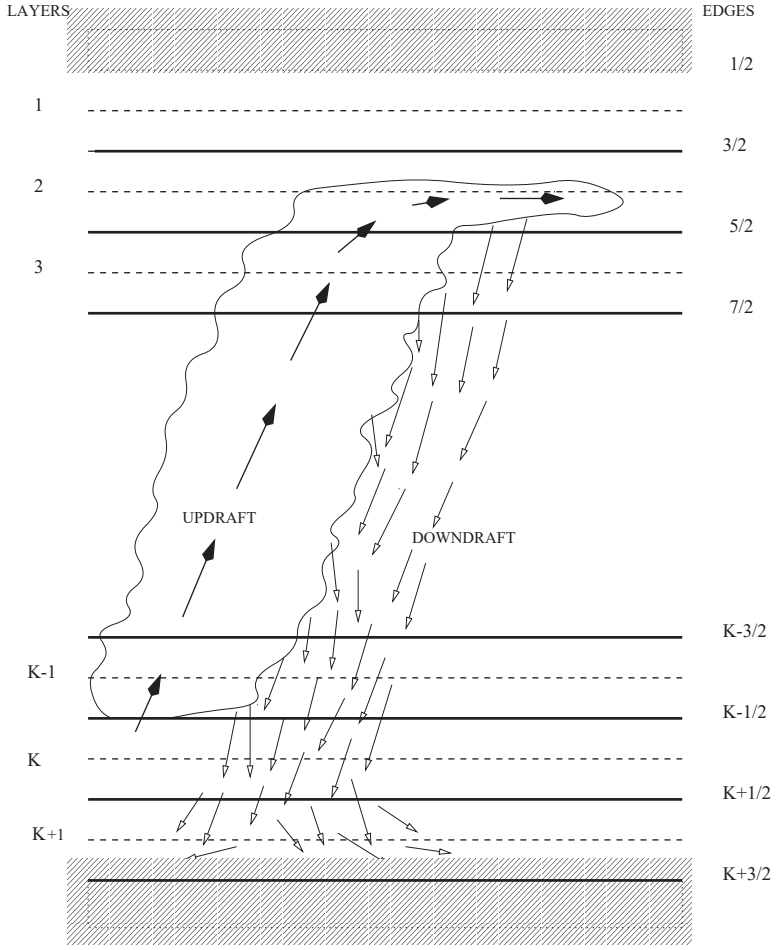

Figure 14: The vertical grid

A schematic of the vertical grid is shown in figure 14 with two subcloud layers and a tilted updraft with an associated downdraft.

We use the same discrete hydrostatic equation used in MS92, but with virtual potential temperature. We define

$$\Delta z_k = z_{k-\frac{1}{2}} - z_{k+\frac{1}{2}} \tag{56}$$

and

$$\Delta p_k = p_{k+\frac{1}{2}} - p_{k-\frac{1}{2}}. \tag{57}$$

a. The Entrainment Relation

Below the updraft top, the normalized mass flux η^u is defined at the layer edges and is assumed to have the form

$$\eta^u_{k-\frac{1}{2}} = 1 + \lambda\zeta_{k-\frac{1}{2}} + \lambda^2\xi_{k-\frac{1}{2}} \tag{58}$$

for $k = i+1, i+2, \ldots, K-1$, where

$$\zeta_{k-\frac{1}{2}} = (z_{k-\frac{1}{2}} - z_B) \tag{59a}$$

and

$$\xi_{k-1/2} = \frac{1}{2}(z_{k-\frac{1}{2}} - z_B)^2, \tag{59b}$$

where, z_B is the height of the top of the subcloud layer. At the updraft top (denoted by integer level i), we define the normalized mass flux as

$$\eta^u_i = 1 + \lambda\zeta_i + \lambda^2\xi_i, \tag{60}$$

where

$$\zeta_i = (z_i - z_B) \tag{61a}$$

and

$$\xi_i = \frac{1}{2}(z_i - z_B)^2. \tag{61b}$$

Then,

$$\eta^u_{k-\frac{1}{2}} = \eta^u_{k+\frac{1}{2}} + \lambda(\zeta_{k-\frac{1}{2}} - \zeta_{k+\frac{1}{2}}) + \lambda^2(\xi_{k-\frac{1}{2}} - \xi_{k+\frac{1}{2}}) \tag{62}$$

and

$$\eta^u_i = \eta^u_{i+\frac{1}{2}} + \lambda(\zeta_i - \zeta_{i+\frac{1}{2}}) + \lambda^2(\xi_i - \xi_{i+\frac{1}{2}}). \tag{63}$$

b. The Condensate Budget and the Entrainment Parameter

The discrete form of the condensate budget (34) can be written as

$$\eta^u_{k-\frac{1}{2}} q^{uC}_{k-\frac{1}{2}} = \eta^u_{k+\frac{1}{2}} q^{uC}_{k+\frac{1}{2}} + \eta^u_{k+\frac{1}{2}} q^u_{k+\frac{1}{2}} - \eta^u_{k-\frac{1}{2}} q^u_{k-\frac{1}{2}} + (\eta^u_{k-\frac{1}{2}} - \eta^u_{k+\frac{1}{2}}) q^T_k - \mathcal{R}_k, \tag{64}$$

for all $k = i+1, \ldots, K-1$, where $\mathcal{R}_k$ is the rate conversion of condensate to rain. When $k = K-1$ in (64), $q^u_{K-\frac{1}{2}} = q_B$, the specific humidity of the subcloud layer air entering the updraft. [5] Similarly, discretizing (34) over the lower half of the top layer of the updraft, between levels i and $i+\frac{1}{2}$, we can write

$$\eta^u_i q^{uC}_i = \eta^u_{i+1/2} q^{uC}_{i+\frac{1}{2}} + \eta^u_{i+\frac{1}{2}} q^u_{i+\frac{1}{2}} - \eta^u_i q^u_i + (\eta^u_i - \eta^u_{i+\frac{1}{2}}) q^T_i - \mathcal{R}_i, \tag{65}$$

where $\mathcal{R}_i$ is the rate conversion of condensate to rain in the top layer. We choose the following form for $\mathcal{R}_k$:

$$\begin{aligned} \mathcal{R}_k &= c^w_0 \left[\tilde{a}_k \left\{ (1 - Q(T^u))\, \eta^u (q^{uC} - q^w_0) \right\}_{k-\frac{1}{2}} + \tilde{b}_k \left\{ (1 - Q(T^u))\, \eta^u (q^{uC} - q^w_0) \right\}_{k+\frac{1}{2}} \right] \\ &+ c^I_0 \left[\tilde{a}_k \left\{ Q(T^u) \eta^u (q^{uC} - q^I_0) \right\}_{k-\frac{1}{2}} + \tilde{b}_k \left\{ Q(T^u) \eta^u (q^{uC} - q^I_0) \right\}_{k+\frac{1}{2}} \right], \end{aligned} \tag{66}$$

for all $k = i+1, \ldots, K-1$, where c^I_0 and c^w_0 are the auto conversion coefficients for ice and water, respectively, $\tilde{a}_k = (p_k - \hat{p}_{k-\frac{1}{2}})/(\hat{p}_{k+\frac{1}{2}} - \hat{p}_{k-\frac{1}{2}})$ and $\tilde{a}_k + \tilde{b}_k = 1$. The term inside the square brackets is an approximation to the term $\eta^u_k q^{uC}_k$ used in Lord's formulation. At the detrainment level i we use

$$\begin{aligned} \mathcal{R}_i &= c^w_0 \left[\tilde{a}_i \left\{ (1 - Q(T^u))\, \eta^u (q^{uC} - q^w_0) \right\}_i + \tilde{b}_i \left\{ (1 - Q(T^u))\, \eta^u (q^{uC} - q^w_0) \right\}_{i+\frac{1}{2}} \right] \\ &+ c^I_0 \left[\tilde{a}_i \left\{ Q(T^u) \eta^u (q^{uC} - q^I_0) \right\}_i + \tilde{b}_i \left\{ Q(T^u) \eta^u (q^{uC} - q^I_0) \right\}_{i+\frac{1}{2}} \right]. \end{aligned} \tag{67}$$

We assume that no cloud condensate enters the updraft through the bottom, *i.e.*, $q^{uC}_{K-\frac{1}{2}} = 0$. Substituting (66) and (67) in (64) and (65), we can write the discrete condensate budget as

$$\begin{aligned} a_k \eta^u_{k-\frac{1}{2}} q^{uC}_{k-\frac{1}{2}} &= b_k \eta^u_{k+\frac{1}{2}} q^{uC}_{k+\frac{1}{2}} + \eta^u_{k+\frac{1}{2}} q^u_{k+\frac{1}{2}} - \eta^u_{k-\frac{1}{2}} q^u_{k-\frac{1}{2}} + (\eta^u_{k-\frac{1}{2}} - \eta^u_{k+\frac{1}{2}}) q^T_k \\ &+ \tilde{b}_k \eta^u_{k+\frac{1}{2}} a^0_{k+\frac{1}{2}} + \tilde{a}_k \eta^u_{k-\frac{1}{2}} a^0_{k-\frac{1}{2}} \end{aligned} \tag{68}$$

where

$$a_k = 1 + \tilde{a}_k \left[c^I_0 Q(T^u_{k+\frac{1}{2}}) + c^w_0 (1 - Q(T^u_{k+\frac{1}{2}})) \right] \Delta z_k, \tag{69a}$$

$$b_k = 1 - \tilde{b}_k \left[c^I_0 Q(T^u_{k+\frac{1}{2}}) + c^w_0 (1 - Q(T^u_{k+\frac{1}{2}})) \right] \Delta z_k, \tag{69b}$$

[5] When there is more than one model layer in the subcloud layer, we need to make some assumption regarding the property of the air entering the updraft through the cloud base. Presently, we are using a mass-weighted mean of the subcloud layer values for both the specific humidity and the moist static energy entering the updraft.

and

$$a^0_{k-\frac{1}{2}} = c^I_0 Q(T^u_{k-\frac{1}{2}})(q^I_0)_{k-\frac{1}{2}} + c^w_0(1 - Q(T^u_{k-\frac{1}{2}}))(q^w_0)_{k-\frac{1}{2}}, \tag{69c}$$

for all $k = i+1, ...K-1$, and

$$\begin{aligned} a_i \eta^u_i q^{uC}_i &= b_i \eta^u_{i+\frac{1}{2}} q^{uC}_{i+\frac{1}{2}} + \eta^u_{i+\frac{1}{2}} q^u_{i+\frac{1}{2}} - \eta^u_i q^u_i + (\eta^u_i - \eta^u_{i+\frac{1}{2}}) q^T_i \\ &+ \tilde{b}_i \eta^u_{i+\frac{1}{2}} a^0_{i+\frac{1}{2}} + \tilde{a}_i \eta^u_i a^0_i \end{aligned} \tag{70}$$

where

$$a_i = 1 + \tilde{a}_i \left[c^I_0 Q(T^u_{i+\frac{1}{2}}) + c^w_0(1 - Q(T^u_{i+\frac{1}{2}})) \right] (z_i - z_{i+\frac{1}{2}}), \tag{71a}$$

$$b_i = 1 - \tilde{b}_i \left[c^I_0 Q(T^u_{i+\frac{1}{2}}) + c^w_0(1 - Q(T^u_{i+\frac{1}{2}})) \right] (z_i - z_{i+\frac{1}{2}}), \tag{71b}$$

and

$$a^0_i = c^I_0 Q(T^u_i)(q^I_0)_i + c^w_0(1 - Q(T^u_i))(q^w_0)_i, \tag{71c}$$

at the updraft top. It should be remarked that the above treatment of the moisture budget within an updraft layer is very simplistic compared to the standard implementation of Arakawa-Schubert as described in CA97b. Nevertheless, it is an improvement over the precipitation formulation in the original RAS, while still retaining the capability to solve for the entrainment parameter in an economical way (by avoiding the iteration needed in the standard implementation).

The discrete form of the updraft moist static energy budget (13) can be written as

$$\eta^u_{k-\frac{1}{2}} h^u_{k-\frac{1}{2}} = h_B + \sum_{K-1}^{k} (\eta^u_{j-\frac{1}{2}} - \eta^u_{j+\frac{1}{2}}) h_j, \tag{72}$$

for all $k = i+1, \ldots, K-1$, and

$$\eta^u_i h^u_i = \eta^u_{i+\frac{1}{2}} h^u_{i+\frac{1}{2}} + (\eta^u_i - \eta^u_{i+\frac{1}{2}}) h_i, \tag{73}$$

at the updraft top. Here, h_B is the subcloud layer's moist static energy, which is entering the updraft from below. Using (72), (25), (8), (58), and (60) in (68) and (70), and after simplification (see MS99 fordetails), we obtain the following quadratic form for the condensate at the updraft detrainment level:

$$\eta^u_i q^{uC}_i = \lambda^2 \tilde{H} + \lambda \tilde{G} + \tilde{F}. \tag{74}$$

Using (74) in the non-buoyancy condition (32) applied at the cloud top and after further manipulations, we can obtain a quadratic equation in the entrainment parameter λ whose coefficients depend only on environmental quantities. Once λ is obtained from this equation, we can obtain the normalized mass flux η^u from (58) and (60), and the cloud moist static energy h^u from (72) and (73). Then using (25), we can obtain q^u, the in-cloud specific humidity, at the updraft top as well as at the layer edges. Subsequently, we can obtain the vertical profiles of the total condensate q^{uC}, cloud suspended liquid water q^{uL} and ice q^{uI}. Then the rain $\mathcal{R}_k$ produced at level k can be obtained from (66) and (67).

c. Calculation of Downdraft Properties

As mentioned before, we have followed the procedure of CA in determining the downdraft properties, with some minor modifications. We have coded the solution procedure such that we can start the downdraft from any level at or below the level of detrainment of the updraft. Discrete forms of the set of downdraft equations (40)-(46) are solved iteratively, one layer at a time, starting from the top of the downdraft. All downdraft properties are calculated at the half-integer levels.

The solution of the discrete form of (45) for the fractional area covered by the downdraft, σ, requires a boundary condition at the top of the downdraft. We simply specify a σ at the top by considering only the tilting term in (45). Thus, if the downdraft calculation starts from the updraft detrainment level i, then we assume:

$$\sigma_i = \left(\frac{2}{\rho^u \pi a} \frac{\eta^u}{w^u} sin\theta \right)_i (z_i - z_{i-\frac{1}{2}}). \tag{75}$$

If the downdraft calculation starts from a level $k + \frac{1}{2}$ below the level i, then we take:

$$\sigma_{k+\frac{1}{2}} = \left(\frac{2}{\rho^u \pi a} \frac{\eta^u}{w^u} sin\theta \right)_{k-\frac{1}{2}} (z_{k-\frac{1}{2}} - z_k) + \left(\frac{2}{\rho^u \pi a} \frac{\eta^u}{w^u} sin\theta \right)_{k-\frac{1}{2}} (z_k - z_{k+\frac{1}{2}}). \tag{76}$$

For levels below the downdraft starting level, we solve (45) by adopting the following

discretization:

$$\sigma_{k+\frac{1}{2}} = \left[\sigma_{k-\frac{1}{2}} + \left\{\frac{V_t^d}{w^d+V_t^d}\left(\frac{2}{\rho^u\pi a}\frac{\eta^u}{w^u}sin\theta\right)\right\}_{k-\frac{1}{2}}(z_k - z_{k-\frac{1}{2}}) + \left\{\frac{V_t^d}{w^d+V_t^d}\left(\frac{2}{\rho^u\pi a}\frac{\eta^u}{w^u}sin\theta\right)\right\}_{k+\frac{1}{2}}(z_{k+\frac{1}{2}} - z_k) - \frac{2}{\left\{\rho^d q_r^d(w^d+V_t^d)\right\}_{k-\frac{1}{2}} + \left\{\rho^d q_r^d(w^d+V_t^d)\right\}_{k+\frac{1}{2}}}(E_r\Delta z)_k\right] \times \left[1 + \frac{1}{\rho^d_{k+\frac{1}{2}}}\frac{1}{(w^d+V_t^d)_{k+\frac{1}{2}}}\left((\rho^d w^d)_{k+\frac{1}{2}} - (\rho^d w^d)_{k-\frac{1}{2}}\right)\right]^{-1}, \tag{77}$$

for $(\rho^d w^d)_{k+\frac{1}{2}}) > (\rho^d w^d)_{k-\frac{1}{2}})$ and

$$\sigma_{k+\frac{1}{2}} = \sigma_{k-\frac{1}{2}} + \left\{\frac{V_t^d}{w^d+V_t^d}\left(\frac{2}{\rho^u\pi a}\frac{\eta^u}{w^u}sin\theta\right)\right\}_{k-\frac{1}{2}}(z_k - z_{k-\frac{1}{2}}) + \left\{\frac{V_t^d}{w^d+V_t^d}\left(\frac{2}{\rho^u\pi a}\frac{\eta^u}{w^u}sin\theta\right)\right\}_{k+\frac{1}{2}}(z_{k+\frac{1}{2}} - z_k) - \frac{2}{\left\{\rho^d q_r^d(w^d+V_t^d)\right\}_{k-\frac{1}{2}} + \left\{\rho^d q_r^d(w^d+V_t^d)\right\}_{k+\frac{1}{2}}}(E_r\Delta z)_k - \frac{\sigma_{k-\frac{1}{2}}}{\rho^d_{k-\frac{1}{2}}}\frac{1}{(w^d+V_t^d)_{k-\frac{1}{2}}}\left((\rho^d w^d)_{k+\frac{1}{2}} - (\rho^d w^d)_{k-\frac{1}{2}}\right), \tag{78}$$

otherwise.

This discretization is simpler than the one used by CA.

Another minor change we have made is to use

$$(\Delta\eta_0)_k = max\left[|\eta^d_{k+\frac{1}{2}} - \eta^d_{k-\frac{1}{2}}|, \frac{\pi\lambda}{2}\eta^u_k(\Delta z)_k\right] \tag{79}$$

in determining the entrainment/detrainment for the downdraft (see page 38 of CA for details). This modification implies that when $|\eta^d_{k+\frac{1}{2}} - \eta^d_{k-\frac{1}{2}}| > \frac{\pi\lambda}{2}\eta^u_k(\Delta z)_k$, there is either entrainment or detrainment based on the sign of $\eta^d_{k+\frac{1}{2}} - \eta^d_{k-\frac{1}{2}}$.

In the CA implementation of the downdraft, each model layer is subdivided into several layers. We perform the downdraft calculation on the original grid assuming

that the vertical resolution is reasonably fine. If the vertical resolution is too coarse, the downdraft calculation may not converge. The mass flux at the downdraft starting level is taken as zero. If the iteration does not converge for the next lower level, then it is assumed that there is no downdraft in that layer and the rain flux is simply added to the next layer without any evaporation. The procedure is repeated for layers below until the either the downdraft stops or reaches the bottom surface. If the downdraft stops before reaching the bottom, another downdraft may start from any layers below. This possibility is also allowed. Unlike CA, we allow the downdraft to penetrate the layers below the cloud base by explicitly calculating the downdraft properties in all subcloud layers including the layer next to the bottom surface. In applying (77) and (78) to levels below the cloud base, we use the fact that there is zero contribution from the tilting term. The downdraft airmass, after impinging on the bottom boundary, is assumed to modify the subcloud layer properties.

We implement this updraft/downdraft scheme one cloud type at a time. As discussed before, the downdraft directly modifies the mass flux kernel of this cloud type. As in the original RAS, interaction between different cloud types is through subsequent calls to other cloud types.

d. Cumulus Effects on the Large-scale Environment

The discrete forms of the budgets of the dry and moist static energies in the environment are written in the form

$$\left(\frac{\partial s_k}{\partial t}\right)_c = M_B \Gamma_s(k), \tag{80}$$

$$\left(\frac{\partial h_k}{\partial t}\right)_c = M_B \Gamma_h(k), \tag{81}$$

where $\Gamma_s(k)$ and $\Gamma_h(k)$ are the rate of change of dry and moist static energies of the environment per unit cloud-base mass flux. In discrete form, they are given by

$$\begin{aligned}
\Gamma_s(k) &= \frac{g}{\Delta p_k}\Big[\eta^u_{k-\frac{1}{2}}(s_{k-\frac{1}{2}} - s_k) + \eta^u_{k+\frac{1}{2}}(s_k - s_{k+\frac{1}{2}}) + \delta_{i,k}\eta^u_i(s^u_i - s_i) \\
&- \delta_{i,k}\beta\eta^u_i(L_c q_i^{uT} + L_f q_i^{uI}) \\
&+ \eta^d_{k-\frac{1}{2}}(s^d_{k-\frac{1}{2}} - s_{k-\frac{1}{2}}) - \eta^d_{k+\frac{1}{2}}(s^d_{k+\frac{1}{2}} - s_{k+\frac{1}{2}}) - L_c(E_r\Delta z)_k\Big],
\end{aligned} \tag{82}$$

and

$$\begin{aligned}\Gamma_h(k) &= \frac{g}{\Delta p_k}\Big[\eta^u_{k-\frac{1}{2}}(h_{k-\frac{1}{2}}-h_k)+\eta^u_{k+\frac{1}{2}}(h_k-h_{k+\frac{1}{2}})+\delta_{i,k}\eta^u_i(h^u_i-h_i)\\ &+ \eta^d_{k-\frac{1}{2}}(h^d_{k-\frac{1}{2}}-h_{k-\frac{1}{2}})-\eta^d_{k+\frac{1}{2}}(h^d_{k+\frac{1}{2}}-h_{k+\frac{1}{2}})\Big], \end{aligned} \tag{83}$$

for $k = i, i+1\ldots., K-1$, and

$$\begin{aligned}\Gamma_s(k) &= \frac{g}{\Delta p_k}\Big[r_k(s_{K-\frac{1}{2}}-s_B+\eta^d_{K+M-\frac{1}{2}}\{s^d_{K+M-\frac{1}{2}}-s_{K+M-\frac{1}{2}}\})\\ &+ \eta^d_{k-\frac{1}{2}}(s^d_{k-\frac{1}{2}}-s_{k-\frac{1}{2}})-\eta^d_{k+\frac{1}{2}}(s^d_{k+\frac{1}{2}}-s_{k+\frac{1}{2}})-L_c(E_r\Delta z)_k\Big], \end{aligned} \tag{84}$$

and

$$\begin{aligned}\Gamma_h(k) &= \frac{g}{\Delta p_k}\Big[r_k(h_{K-\frac{1}{2}}-h_B+\eta^d_{K+M-\frac{1}{2}}\{h^d_{K+M-\frac{1}{2}}-h_{K+M-\frac{1}{2}}\})\\ &+ \eta^d_{k-\frac{1}{2}}(h^d_{k-\frac{1}{2}}-h_{k-\frac{1}{2}})-\eta^d_{k+\frac{1}{2}}(h^d_{k+\frac{1}{2}}-h_{k+\frac{1}{2}})\Big], \end{aligned} \tag{85}$$

for $k = K, K+1\ldots., K+M-1$, where

$$r_k = \frac{\Delta p_k}{p_{K+M-\frac{1}{2}}-p_{K-\frac{1}{2}}}. \tag{86}$$

Here $\eta^d_{k-\frac{1}{2}}$ is the downdraft mass flux at level $k-\frac{1}{2}$ per unit cloud-base updraft mass flux M_B, $s^d_{k-\frac{1}{2}}$ and $h^d_{k-\frac{1}{2}}$ are the dry and moist static energies in the downdraft, $(E_r\Delta z)_k$ is the normalized rain evaporation rate in layer k in the downdraft, and $\delta_{i,k}$ is the Kronecker delta. The terms with $\delta_{i,k}$ represent detrainment effects, which occur only in the cloud top layer. If we allow for detrainment from other layers, then these equations need to be modified. Also, note that in (82) and (83) we have used $\eta_{i-\frac{1}{2}} = 0$. Below the cloud-base, the subcloud layer is treated as a single layer as far as the updraft effects are concerned (see (84) and (85)). Thus all layers in the subcloud layer experience equal changes due to updraft effects. The downdraft effects are computed individually for all layers in the subcloud layer. In (84) and (85), s_B and h_B are the subcloud layer values of dry and moist static energies entering the updraft. We have also assumed that the downdraft airmass, after impinging on the bottom boundary, mixes within the subcloud layer and the corresponding terms are also included in (84) and (85).

Similar equations can be written for the rate of change of environmental liquid water and ice:

$$\Gamma_L(k) = \frac{g}{\Delta p_k}\left[\eta^u_{k-\frac{1}{2}}(q^L_{k-\frac{1}{2}} - q^L_k) + \eta^u_{k+\frac{1}{2}}(q^L_k - q^L_{k+\frac{1}{2}}) + \delta^k_i \eta^u_i(\{1-\beta\}q^{uL}_i - q^L_i)\right] \quad (87)$$

and

$$\Gamma_I(k) = \frac{g}{\Delta p_k}\left[\eta^u_{k-\frac{1}{2}}(q^I_{k-\frac{1}{2}} - q^I_k) + \eta^u_{k+\frac{1}{2}}(q^I_k - q^I_{k+\frac{1}{2}}) + \delta^k_i \eta^u_i(\{1-\beta\}q^{uI}_i - q^I_i)\right] \quad (88)$$

for $k = i, i+1, \ldots, K-1$, where we have ignored the downdraft effects. [6]

From (82), (83) and (88), we can obtain the rate of change of temperature and moisture due to cumulus effects as

$$\left(\frac{\partial T_k}{\partial t}\right)_c = \frac{M_B}{c_p}\,\Gamma_s(k), \quad (89)$$

and

$$\left(\frac{\partial q_k}{\partial t}\right)_c = \frac{M_B}{L_c}\,\left[\Gamma_h(k) - \Gamma_s(k) + L_f\Gamma_I(k)\right]. \quad (90)$$

e. The Cloud Work Function, Mass-flux Kernel and Cloud Base Mass Flux

Once we have determined the entrainment parameter, the normalized mass flux, vertical profiles of cloud moist static energy, and total water and its components, we can calculate the cloud work function. We discretize (31) as follows:

$$\begin{aligned}\mathcal{A}_i = \sum_{K-1}^{i+1} \frac{1}{\tilde{L}_k}\Big[&\left(h^u_{k-\frac{1}{2}} + L_f q^{uI}_{k-\frac{1}{2}} - h^{**}_k - \tilde{L}_k(q^{uC}_{k-\frac{1}{2}} - q^L_k - q^I_k)\right)\eta^u_{k-\frac{1}{2}}(\phi_{k-\frac{1}{2}} - \phi_k) \\ &+ \left(h^u_{k+\frac{1}{2}} + L_f q^{uI}_{k+\frac{1}{2}} - h^{**}_k - \tilde{L}_k(q^{uC}_{k+\frac{1}{2}} - q^L_k - q^I_k)\right)\eta^u_{k+\frac{1}{2}}(\phi_k - \phi_{k+\frac{1}{2}})\Big] \\ +\frac{1}{2\tilde{L}_i}\Big[&h^u_{i+\frac{1}{2}} + L_f q^{uI}_{i+\frac{1}{2}} - h^{**}_{i+\frac{1}{2}} - \tilde{L}_{i+\frac{1}{2}}(q^{uC}_{i+\frac{1}{2}} - q^L_{i+\frac{1}{2}} - q^I_{i+\frac{1}{2}})\Big]\,\eta^u_{i+\frac{1}{2}}(\phi_i - \phi_{i+\frac{1}{2}}). \quad (91)\end{aligned}$$

[6] During our testing with this discretization for the liquid water and ice, we discovered that it can easily produce negative values, since the scheme is not positive definite and the condensate field can be highly discontinuous in the vertical. Because of this, in the results presented in this paper, we ignore the condensate in the environment. Then (87) and (88) will have non-zero values only at the detrainment level. Neglect of environmental condensate implies that cloud types cannot recognize the condensate in the environment detrained by the previously invoked cloud types. We do not view this as a serious limitation.

The values of $h^{**}_{i+\frac{1}{2}}$, $\tilde{L}_{i+\frac{1}{2}}$, $q^L_{i+\frac{1}{2}}$, and $q^I_{i+\frac{1}{2}}$ in (91) are taken as averages of those at integer levels i and $i+1$.

As in CA97b, we have not included downdraft effects in the calculation of the cloud work function. Justification for doing so is provided by CA97a. Following the procedure described in subsection 5.2, we calculate $\mathcal{K}_i$ numerically using (91). If $\mathcal{K}_i$ is positive, then such a cloud type cannot exist. The large-scale forcing can be computed from the cloud work function as described in MS92. Once the kernel and the large-scale forcing is known, the cloud-base mass flux and the adjustments to the large-scale environment can be calculated.

REFERENCES

Arakawa, A., and W. H. Schubert, 1974: Interaction of a cumulus cloud ensemble with the large-scale environment. Part I. *J. Atmos. Sci..*, **31**, 674-701.

Arakawa, A., and M.-D. Cheng, 1993: The Arakawa-Schubert cumulus parameterization *The representation of cumulus convection in numerical models of the atmosphere*, K. A. Emanuel and D. J. Raymond, Ed. American Meteorological Society, 123-136.

Arakawa, A., and C. M. Wu, 2013: A unified representation of deep moist convecion in numerical modeling of the atmosphere. Part I. *J. Atmos. Sci..*, **70**, 1977-1992.

Bogenschutz, P. A. and S. K. Krueger:2013: A simplified PDF parameterization of subgrid-scale clouds and turbulence for cloud-resolving models. *JAMES*, **5**, 195-211.

Cheng, M.-D., 1989: Effects of downdrafts and mesoscale convective organization on the heat and moisture budgets of tropical cloud clusters. Part I: A diagnostic cumulus ensemble model. *J. Atmos. Sci..*, **46**, 1517-1538.

Cheng, M.-D., and A. Arakawa, 1997a: Inclusion of rain water budget and convective

downdrafts in the Arakawa-Schubert cumulus parameterization. *J. Atmos. Sci..*, **54**, 1359-1378.

Cheng, M.-D., and A. Arakawa, 1997b: Computational procedures for the Arakawa-Schubert cumulus parameterization: Tech. Rep. No. 101, Department of Atmospheric Sciences, University of California, Los Angeles, pp 50.

Cox, S. K., and K. T. Griffith, 1978: Tropospheric radiative divergence during Phase III of GARP Atlantic Tropical Experiment (GATE). Atmos. Sci. Paper No.291 Colorado State University, 166pp.

Gettelman, A., H. Morrison, K. Thayer-Calder, and C. M. Zarzycki, 2019: The impact of rimed ice hydrometeors on global and regional climate. *JAMES*, **11**, 1543-1562.

Han, J., W. Wang, Y. C. Kwon, S.-Y. Hong, V. Tallapragada, and F. Yang, 2017: Updates in the NCEP GFS cumulus convection schemes with scale and aerosol awareness. *Wea. Forecasting*, **33**, 2005-2017.

Hong, S-Y., and H. L. Pan, 1996: Nonlocal boundary layer vertical diffusion in a medium-range forecast model. *Mon. Wea. Rev..*, **124**, 2322-2339.

Hou, Y.-T., K. A. Campana, and S.-K. Yang, 1996: Shortwave radiation calculations in the NCEP global model. International Radiation Symposium, Aug. 18-24, 1996, Fairbanks, Alaska.

Kao, C. Y. J., and Y. Ogura, 1987: Response of cumulus clouds to large-scale forcing using the Arakawa-Schubert cumulus parameterization. *J. Atmos. Sci..*, **44**, 2437-2458.

Krishnamurti, T. N., Y. Ramanathan, H.-L. Pan, R. J. Pasch, and J. Molinari, 1980: Cumulus parameterization and rainfall rates I. *Mon. Wea. Rev..*, **108**, 465-472.

Lord, S. J., 1978: Development and observational verification of a cumulus cloud parameterization. Ph.D. dissertation, University of California, Los Angeles,

359 pp.

Lord, S. J., 1982: Interaction of a cumulus cloud ensemble with the large-scale environment. Part III: Semiprognostic test of the Arakawa-Schubert cumulus parameterization. *J. Atmos. Sci..*, **39**, 88-103.

Lord, S. J., W. C. Chao, and A. Arakawa, 1982: Interaction of a cumulus cloud ensemble with the large-scale environment. Part IV: The discrete model. *J. Atmos. Sci..*, **39**, 104-113.

Moorthi, S., 1997: NWP experiments with a semi-Lagrangian semi-implicit global model at NCEP. *Mon. Wea. Rev..*, **120**, 978-1002.

Moorthi, S., 2000: Application of Relaxed Arakawa-Schubert cumulus parameterization to the NCEP climate model - some sensitivity experiments. *General Circulation Modeling: Past, Present and Future*, Ed. David Randall, Publisher: Academic Press.

Moorthi, S., and M.J. Suarez, 1992: Relaxed Arakawa-Schubert: A parameterization of moist convection for general circulation models. *Mon. Wea. Rev..*, **120**, 978-1002.

Moorthi, S., and M.J. Suarez, 1999: Documentation of version 2 of relaxed Arakawa-Schubert cumulus parameterization with convective downdrafts. *NOAA Tech. Rep. # NWS/NCEP 99-01*, 44pp.

Pan, H.-L. and W.-S. Wu, 1995: Implementing a Mass Flux Convection Parameterization Package for the NMC Medium-Range Forecast Model. NMC Office Note, No. 409, 40pp. [Available from NCEP, 5200 Auth Road, Washington, DC 20233

Simpson, J. and V. Wiggert, 1969: Models of precipitating cumulus towers. *Mon. Wea. Rev..*, **97**, 471-489.

Stefanova, L, et al, 2022: Description and Results from UFS Coupled Prototypes for Future Global, Ensemble and Seasonal Forecasts at NCEP. Office note (Na-

tional Centers for Environmental Prediction (U.S.)) ; 510,
DOI : https://doi.org/10.25923/knx kz26 pp 201.

Sud, Y., and A. Mood, 1988: The roles of dry convection, cloud-radiation feedback processes, and the influence of recent improvements in the parameterization of convection in the GLA GCM. *Mon. Wea. Rev..*, **116**, 2366-2387.

Sud, Y., and G. K. Walker, 1993: A rain evaporation and downdraft prarameterization to complement a cumulus updraft scheme and it evaluation using GATE data. *Mon. Wea. Rev..*, **121**, 3019-3039.

Sud, Y., and G. K. Walker, 1999a: Microphysics of clouds with the relaxed Arakawa-Schubert Scheme (McRAS). Part I: Design and evaluation with GATE Phase III data. *J. Atmos. Sci..*, **56**, 3196-3220.

Sud, Y., and G. K. Walker, 1999b: Microphysics of clouds with the relaxed Arakawa-Schubert Scheme (McRAS). Part II: Implementation and performance in GEOS II GCM. *J. Atmos. Sci..*, **56**, 3221-3240.

Thompson R. M., Jr., S. W. Payne, E. E. Recker, and R. J. Reed, 1979: Structure and properties of synoptic-scale wave disturbances in the intertropical convergence zone of the eastern Atlantic. *J. Atmos. Sci..*, **36**, 53-72.

Thuburn J 1996: TVD schemes, positive schemes, and the universal limiter. *Mon. Wea. Rev.,*, **125**, 1990-1993.

Yanai, M., S. K. Esbensen, and J. H. Chu, 1973: Determination of bulk properties of tropical cloud clusters from large-scale heat and moisture budgets. *J. Atmos. Sci..*, **30**, 611-627.